ISSN 1560-3547, Regular and Chaotic Dynamics, 2018, Vol. 23, Nos. 7–8, pp. 908–932. © Pleiades Publishing, Ltd., 2018.

Lyapunov Analysis of Strange Pseudohyperbolic Attractors: Angles Between Tangent Subspaces, Local Volume Expansion and Contraction

Pavel V. Kuptsov[1*] and Sergey P. Kuznetsov[2,3]**

[1] *Institute of electronics and mechanical engineering, Yuri Gagarin State Technical University of Saratov ul. Politekhnicheskaya 77, Saratov, 410054 Russia*

[2] *Udmurt State University ul. Universitetskaya 1, Izhevsk, 426034 Russia*

[3] *Kotel'nikov's Institute of Radio-Engineering and Electronics of RAS, Saratov Branch ul. Zelenaya 38, Saratov, 410019 Russia*

Received September 07, 2018; accepted November 06, 2018

Abstract—Pseudohyperbolic attractors are genuine strange chaotic attractors. They do not contain stable periodic orbits and are robust in the sense that such orbits do not appear under variations. The tangent space of these attractors is split into a direct sum of volume expanding and contracting subspaces and these subspaces never have tangencies with each other. Any contraction in the first subspace, if it occurs, is weaker than contractions in the second one. In this paper we analyze the local structure of several chaotic attractors recently suggested in the literature as pseudohyperbolic. The absence of tangencies and thus the presence of the pseudohyperbolicity is verified using the method of angles that includes computation of distributions of the angles between the corresponding tangent subspaces. Also, we analyze how volume expansion in the first subspace and the contraction in the second one occurs locally. For this purpose we introduce a family of instant Lyapunov exponents. Unlike the well-known finite time ones, the instant Lyapunov exponents show expansion or contraction on infinitesimal time intervals. Two types of instant Lyapunov exponents are defined. One is related to ordinary finite-time Lyapunov exponents computed in the course of standard algorithm for Lyapunov exponents. Their sums reveal instant volume expanding properties. The second type of instant Lyapunov exponents shows how covariant Lyapunov vectors grow or decay on infinitesimal time. Using both instant and finite-time Lyapunov exponents, we demonstrate that average expanding and contracting properties specific to pseudohyperbolicity are typically violated on infinitesimal time. Instantly volumes from the first subspace can sometimes be contacted, directions in the second subspace can sometimes be expanded, and the instant contraction in the first subspace can sometimes be stronger than the contraction in the second subspace.

MSC2010 numbers: 37D45,37D30,37D25,65L99,34D08

DOI: 10.1134/S1560354718070079

Keywords: chaotic attractor, strange pseudohyperbolic attractor, method of angles, hyperbolic isolation, Lyapunov exponents, finite-time Lyapunov exponents, instant Lyapunov exponents, covariant Lyapunov vectors

INTRODUCTION

Success in practical applications of chaotic theory essentially depends on the robustness of the implemented systems. This means that the chaotic regime must not be destroyed or qualitatively changed under small variations of parameters of the system [26]. Moreover, the chaotic regime has to demonstrate good stochastic properties proven by rigorous mathematical analysis.

*E-mail: p.kuptsov@rambler.ru

**E-mail: spkuz@yandex.ru

One class satisfying these requirements contains systems with uniformly hyperbolic chaos. Systems of this type, such as the Smale – Williams solenoid, manifest deterministic chaos justified in a rigorous mathematical sense. They demonstrate strong and structurally stable stochastic properties [12, 38, 39]. Though hyperbolic attractors were regarded for many years only as a mathematical abstraction, many examples of physically realizable systems with a hyperbolic attractor have recently been suggested [16, 17].

Uniformly hyperbolic attractors contain only saddle trajectories. For discrete-time systems these trajectories have well-defined contracting and expanding manifolds. The former contains phase trajectories approaching the attractor in direct time and the latter corresponds to the approaching in reversed time. In the linear space of small perturbations tangent to these manifolds this situation corresponds to the splitting of the whole space into a direct sum of two subspaces such that in one of them all directions are expanding and in the second one they are contracting. The important feature of the saddle trajectories and thus of the hyperbolic attractors is that the contracting and expanding manifolds can intersect each other but can not have tangencies. In the associated tangent space it is reflected in the absence of clashes between vectors from the expanding and contracting subspaces so that the angles between these subspaces never vanish. For systems with continuous time in addition to the expanding and contracting tangent subspaces the neutral tangent subspace is added, and all these three subspaces never have tangencies with each other.

Besides the uniformly hyperbolic attractors one more class of systems with a "good" chaos is formed by systems with pseudohyperbolic attractors (the Lorenz attractor, "wild" attractors) [7, 25, 27, 28]. These attractors are genuine strange attractors since each orbit has positive Lyapunov exponent, i. e., stable periodic orbits are absent, and this property is robust being preserved under at least small perturbations. The tangent space of pseudohyperbolic systems is split into a direct sum of volume expanding and contracting subspaces. Notice that now only the expansion of volumes is required instead of expansion along all direction needed for the uniform hyperbolicity. These splitting must be invariant in time and the subspaces cannot have tangencies.

A necessary condition for the existence of the pseudohyperbolic attractor is the following relation for its Lyapunov exponents [25, 27]:

$$\sum_{i=1}^{n} \lambda_i > 0, \quad \text{and} \quad \lambda_i < 0 \text{ for } i > n. \tag{0.1}$$

Here n is the largest value for which this condition holds. To confirm the pseudohyperbolicity, one also has to ensure that the n-dimensional volume expanding subspace and the $(N-n)$-dimensional contracting subspace have no tangencies.

Based on discussions in [8, 25, 27, 28], the following list of properties of pseudohyperbolic attractors can be formulated:

(i) The tangent space is split into a direct sum of two hyperbolically isolated subspaces such that the angles between them never vanish.

(ii) The first n-dimensional subspace exponentially expands n-dimensional volumes, i. e., the sum of the Lyapunov exponents corresponding to this subspace is positive.

(iii) The second subspace exponentially contracts all its vectors, i. e., all corresponding Lyapunov exponents are negative.

(iv) Any contraction in the first subspace, if it occurs, is exponentially weaker than any contraction in the second subspace.

In this paper we will test these properties for several concrete examples of chaotic systems. The absence of the tangencies (property (i)) will be verified numerically using the implementation of the method of angles as suggested in [13]. Three other properties are satisfied automatically if the necessary condition (0.1) holds. However, unlike the angles that are computed at the trajectory points with small step and thus describe the attractor locally, Lyapunov exponents provide global characteristics and ignore its fine details due to averaging. In this paper we are going to test how the properties (ii), (iii), and (iv) are satisfied locally, on infinitesimal and short time intervals.

For this purpose, finite-time Lyapunov exponents will be computed based both on orthogonal Gram – Schmidt vectors and on covariant Lyapunov vectors. Moreover, instant Lyapunov exponents will be introduced which provide expansion or contraction rates on infinitesimal time.

The paper is organized as follows. In Section 1 we briefly review the methods of computation of Lyapunov exponents, covariant and orthogonal Lyapunov vectors, finite-time Lyapunov exponents. Also, instant Lyapunov exponents are defined. The main section (Section 2) is devoted to the testing of pseudohyperbolicity of several attractors. Finally, in Section 3 the results are discussed.

1. SOME BASICS OF LYAPUNOV ANALYSIS

In this section we briefly review methods of Lyapunov analysis required for the further investigation of pseudohyperbolicity. We discuss the methods of computation of Lyapunov exponents, finite-time exponents, covariant Lyapunov vectors (CLVs), and angles between tangent subspaces. Moreover, we introduce a family of instant Lyapunov exponents that show the exponential growth rates in tangent space on infinitesimal time.

1.1. Covariant Lyapunov Vectors and Angles Between Tangent Subspaces

Computation of angles between tangent subspaces can be done using CLVs. These vectors are named "covariant" since the nth vector at time t_1 is mapped by a tangent flow to the nth vector at time t_2, and a rate of its exponential expansion or contraction averaged over an infinitely long trajectory is equal to the nth Lyapunov exponent λ_n. Two algorithms for computation of these vectors were first reported in the pioneering works [10, 23]. See also the paper [15] for a more detailed explanation and one more algorithm, and also the book [22] for a survey.

The importance of CLVs lies in the fact that they form a tangent basis for expanding and contracting manifolds of trajectories of a dynamical system. In particular, these vectors can indicate hyperbolicity of chaos. By definition, both uniform hyperbolicity and its weaker forms are related to the transversality of the tangent subspaces [7, 12, 21, 38, 39]. A chaotic system is uniformly hyperbolic when expanding, contracting, and also neutral, if any, subspaces are hyperbolically isolated, i.e., never have tangencies. In terms of CLVs this means that the angles between the subspaces spanned by the corresponding CLVs never vanish. In this paper we give attention to the pseudohyperbolicity which requires the absence of tangencies between volume expanding and contracting subspaces [8, 25, 27, 28].

Verification of the hyperbolic isolation of tangent subspaces will be done using the method of angles [13], which in turn is based on the method for CLVs computation suggested in [15] as the LU-method.

Consider a continuous-time system

$$\dot{X}(t) = F\big(X(t), t\big), \tag{1.1}$$

where $X \in \mathbb{R}^N$ is the N-dimensional state vector, and F is a nonlinear function. Infinitely small or tangent perturbations to trajectories of the system (1.1) obey the variational equation

$$\dot{x}(t) = \mathbf{J}(t)x(t), \tag{1.2}$$

where $x \in \mathbb{R}^N$ is a tangent vector and $\mathbf{J}(t) \in \mathbb{R}^{N\times N}$ is the Jacobian matrix, i. e., the matrix of derivatives of F with respect to X. Its time dependence can be both implicit via $X(t)$ and explicit (for the nonautonomous case). For a discrete-time system we have

$$X_{n+1} = F(X_n, n), \tag{1.3}$$

$$x_{n+1} = \mathbf{J}_n x_n. \tag{1.4}$$

Here all terms have the same meaning as above, and n denotes discrete time.

Both for continuous- and discrete-time systems the evolution of the tangent vectors from time t_1 to time t_2 can be expressed as follows:

$$x(t_2) = \boldsymbol{\mathcal{F}}(t_1, t_2)x(t_1), \tag{1.5}$$

where $\boldsymbol{\mathcal{F}}(t_1, t_2)$ is a linear operator called propagator. For discrete-time systems this is merely $t_2 - t_1$ times iterated Jacobian matrix of the system, and for continuous-time systems the propagator is

built from a Jacobian matrix using the Magnus expansion [15]. In numerical simulations the action of the propagator $\boldsymbol{\mathcal{F}}(t_1, t_2)$ is equivalent to solving the variational equation (1.2) or (1.4) from t_1 to t_2 simultaneously with the basic system (1.1) or (1.3), respectively.

Computation routines for Lyapunov exponents and CLVs use inner products of tangent vectors. Its particular form can be chosen arbitrarily, and Lyapunov exponents as well as CLVs do not depend on this choice. However, in some cases, finding an appropriate form for the inner product is important for clarifying the correspondence between mathematical models and numerical approximations. For example, in [3, 14] a special form of the inner product is introduced for analysis of hyperbolicity of chaos in time-delay systems. In our analysis, however, it is enough to consider the simplest standard dot product.

Discussed algorithms for CLVs and angles are based on the standard algorithm for Lyapunov exponents created independently and simultaneously by Benettin et al. [9] and by Shimada and Nagashima [19]. Assume we need to compute K Lyapunov exponents, or CLVs, or going to evaluate first K angles between the tangent subspaces. First, we initialize a set of K unit random tangent vectors orthogonal to each other and gather them as columns of a matrix $\mathbf{Q}_{\mathrm{b}}(t_1)$. Applying the propagator $\boldsymbol{\mathcal{F}}(t_1, t_2)$ to this matrix, we obtain a set of vectors $\widetilde{\mathbf{Q}}_{\mathrm{b}}(t_2)$, now nonorthogonal. We recall that in practice this merely means that we solve variational equations from t_1 to t_2 K times (for each column of $\mathbf{Q}_{\mathrm{b}}(t_1)$). Now we need to orthogonalize $\widetilde{\mathbf{Q}}_{\mathrm{b}}(t_2)$. There are many algorithms to do it. The best known is called the Gram – Schmidt orthogonalization. In more general form this procedure is referred to as QR factorization and consists in representation of the matrix as a product of an orthogonal $\mathbf{Q}$ and an upper triangular $\mathbf{R}$ matrix [11, 20]. Thus, one iteration of the standard algorithm includes the following operations:

$$\boldsymbol{\mathcal{F}}(t_1, t_2)\mathbf{Q}_{\mathrm{b}}(t_1) = \widetilde{\mathbf{Q}}_{\mathrm{b}}(t_2), \tag{1.6}$$

$$\widetilde{\mathbf{Q}}_{\mathrm{b}}(t_2) = \mathbf{Q}_{\mathrm{b}}(t_2)\mathbf{R}_{\mathrm{b}}(t_1, t_2). \tag{1.7}$$

The orthogonal matrix $\mathbf{Q}_{\mathrm{b}}(t_2)$ is used for the next stage of the algorithm.

After skipping some transient, we can consider logarithms of diagonal elements of $\mathbf{R}_{\mathrm{b}}(t_1, t_2)$. Dividing them by the corresponding time step, $\tau = t_2 - t_1$, we obtain finite-time Lyapunov exponents (FTLEs) associated with the time interval τ, and averaging them over a long trajectory we obtain numerical approximations for global Lyapunov exponents λ_i. In what follows, λ_i will be referred to as merely Lyapunov exponents.

The algorithm for CLVs and angles that we use here requires the matrix $\mathbf{Q}_{\mathrm{b}}(t)$. After the transient, the columns of this orthogonal matrix turns to the backward Lyapunov vectors. This name seems to be counterintuitive, but its origin is not related to the direction of iterations in time. It indicates that they have arrived at the current point after a long evolution initialized in the far past [15, 18]. Also, these vectors are known as Gram – Schmidt vectors. The directions pointed by these vectors, except for the first one, depend on the choice of the inner product. This means that individually they do not give much information about the tangent space structure. But the subspaces they span do. Assume that we have already found CLVs and they are gathered as columns of the matrix $\boldsymbol{\Gamma}(t)$. The backward Lyapunov vectors form an orthogonal matrix in the QR-decomposition of $\boldsymbol{\Gamma}(t)$ [15]:

$$\boldsymbol{\Gamma}(t) = \mathbf{Q}_{\mathrm{b}}(t)\mathbf{A}_{\mathrm{b}}(t), \tag{1.8}$$

where $\mathbf{A}_{\mathrm{b}}(t)$ is an upper triangular matrix. Since QR-decomposition preserves subspaces spanned by vector-columns of the decomposed matrix (see, for example, the book [11] for details), Eq. (1.8) shows that the first CLV coincides with the first backward Lyapunov vector, the second one lies in a plane spanned by the first two backward vectors, the third one belongs to a three-dimensional space of the first three backward vectors and so on.

The second part of the algorithm under discussion includes iterations with the adjoint propagator. Notice that the action of the adjoint propagator as well as the action of the inverted one corresponds to steps backward in time [15]. The form of the adjoint propagator depends on the chosen inner product [3, 14], and the standard dot product produces its simplest version: the adjoint propagator is obtained from the original one simply by transposition as $\boldsymbol{\mathcal{F}}^{\mathrm{T}}(t_1, t_2)$. The steps

are performed again with K vectors that are QR-decomposed after each action of the propagator $\boldsymbol{\mathcal{F}}^{\mathrm{T}}(t_1, t_2)$:

$$\boldsymbol{\mathcal{F}}(t_1, t_2)^{\mathrm{T}}\mathbf{Q}_{\mathrm{f}}(t_2) = \widetilde{\mathbf{Q}}_{\mathrm{f}}(t_1), \tag{1.9}$$

$$\widetilde{\mathbf{Q}}_{\mathrm{f}}(t_1) = \mathbf{Q}_{\mathrm{f}}(t_1)\mathbf{R}_{\mathrm{f}}(t_1, t_2). \tag{1.10}$$

Here $\mathbf{Q}_{\mathrm{f}}(t)$ is an orthogonal matrix with K columns. When one drops out some transient, columns of $\mathbf{Q}_{\mathrm{f}}(t)$ become the so-called forward Lyapunov vectors. Here "forward" indicates that the vectors arrive from a far future.

Assume for a moment that we have the full set of N forward vectors. Then the matrix $\mathbf{Q}_{\mathrm{f}}(t)$ is an orthogonal matrix in the QL-decomposition of the CLVs matrix $\boldsymbol{\Gamma}(t)$:

$$\boldsymbol{\Gamma}(t) = \mathbf{Q}_{\mathrm{f}}(t)\mathbf{A}_{\mathrm{f}}(t). \tag{1.11}$$

Here $\mathbf{A}_{\mathrm{f}}(t)$ is a lower triangular matrix [15]. Thus, the Nth forward vector coincides with the last CLV, the last two forward vectors span the subspace containing the $(N-1)$th CLV, and so on. This means that the remaining forward vectors, i. e., the columns of $\mathbf{Q}_{\mathrm{f}}(t)$ from the 1st to the nth, form an orthogonal complement for the subspace containing the last $N-n$ CLVs. Thus, given K backward Lyapunov vectors in $\mathbf{Q}_{\mathrm{b}}(t)$ and K forward Lyapunov vectors in $\mathbf{Q}_{\mathrm{f}}(t)$, we have a subspace with the first K CLVs and an orthogonal complement for the subspace for $N-K$ remaining CLVs. It is enough to compute K CLVs and a series of angles between the subspaces spanned by these vectors.

Equating the left-hand sides of Eqs. (1.8) and (1.11), we obtain

$$\mathbf{P}(t) = [\mathbf{Q}_{\mathrm{f}}(t)]^{\mathrm{T}}\mathbf{Q}_{\mathrm{b}}(t), \tag{1.12}$$

$$\mathbf{P}(t)\mathbf{A}_{\mathrm{b}}(t) = \mathbf{A}_{\mathrm{f}}(t). \tag{1.13}$$

Thus, given $\mathbf{Q}_{\mathrm{b}}(t)$ and $\mathbf{Q}_{\mathrm{f}}(t)$, we first compute $\mathbf{P}(t)$ with Eq. (1.12). Then, since $\mathbf{A}_{\mathrm{b}}(t)$ and $\mathbf{A}_{\mathrm{f}}(t)$ are upper and lower triangular matrices, respectively, they are computed for $\mathbf{P}(t)$ from Eq. (1.13) as its LU decomposition, see [15] for more details. Finally, using $\mathbf{A}_{\mathrm{b}}(t)$ and $\mathbf{Q}_{\mathrm{b}}(t)$ we can find CLVs from Eq. (1.8).

The angles between subspaces are called principal angles. The cosines of these angles can be found as singular values of a matrix whose elements are pairwise inner products of orthogonal basis vectors for these subspaces [11]. We have an orthogonal basis for the first subspace of interest in $\mathbf{Q}_{\mathrm{b}}(t)$, also, there is a basis for the orthogonal complement of the second subspace in $\mathbf{Q}_{\mathrm{f}}(t)$, and $\mathbf{P}(t)$ is the matrix of their inner products. Two n-dimensional subspaces have n principal angles. But since we are interested in verification of tangencies of these subspaces, we need only one of the angles. Because $\mathbf{Q}_{\mathrm{f}}(t)$ is the orthogonal complement to the subspace of interest, the tangency is signaled by the largest principal angle that corresponds to the smallest singular value. Once the matrix $\mathbf{P}$ is computed, we can evaluate a series of K angles. Taking top left square submatrices $\mathbf{P}[1\colon n, 1\colon n]$, where $n = 1, 2, \ldots, K$, and finding their smallest singular values σ_n, we obtain the angle between the n-dimensional subspace of the first CLVs and the $(N-n)$-dimensional subspace of the remaining CLVs as:

$$\theta_n = \pi/2 - \arccos\sigma_n. \tag{1.14}$$

The smallest singular value σ_n, as well as the angle θ_n, vanishes when a tangency between the corresponding subspaces occurs. Because trajectories with the exact tangencies are rather untypical, in actual computations we register a tangency between subspaces if the corresponding angle can be arbitrarily small.

1.2. Finite-time Lyapunov Exponents

Finite-time Lyapunov exponents (FTLEs) characterize expansions and contractions in phase space on finite-time intervals. They are obtained from logarithms of diagonal elements of the upper triangular matrix $\mathbf{R}_{\mathrm{b}}(t_1, t_2)$ computed after each QR decomposition in the course of computation of Lyapunov exponents, see Eq. (1.7):

$$\bar{\Lambda}_n(t_1, t_2) = \frac{\log r_{nn}(t_1, t_2)}{t_2 - t_1}. \tag{1.15}$$

The Lyapunov exponents λ_n are the averagings of FTLEs $\bar{\Lambda}_n(t_1, t_2)$ over an infinitely long trajectory. They always appear in a descending order in computations and show a hierarchy of expansions and contractions in phase space.

The individual meaning of FTLEs (1.15), except for the first one, is not so clear. The first FTLE shows how a typical tangent vector exponentially grows from t_1 to t_2. By construction, the second FTLE is the rate of exponential growth along a direction perpendicular to the fastest one. It does not have much physical meaning in itself. However, the sum $\bar{\Lambda}_1(t_1, t_2) + \bar{\Lambda}_2(t_1, t_2)$ shows the exponential grows rate of a typical two-dimensional area. Similarly, the third FTLE $\bar{\Lambda}_3(t_1, t_2)$ admits a clear interpretation summed with two previous ones: this sum indicates the rate of exponential growth of a typical three-dimensional volume. The sum of the first n FTLEs is a growth rate for a typical n-dimensional volume in the tangent space.

When CLVs became available due to the effective algorithms for their computations [10, 23], in addition to FTLEs (1.15), a new sort of finite-time Lyapunov exponents were introduced, computed as rates of exponential grows of CLVs on the time interval $t_2 - t_1$, see [15]. We will refer to them as FTCLE and denote as $\bar{\mathcal{L}}_n(t_1, t_2)$. Similar to FTLEs (1.15), these CLV based exponents also converge to Lyapunov exponents on large times, but their meaning is different. Each FTCLE characterizes an exponential expansion or contraction rate along a covariant direction where on average the expansion or contraction occurs according to the respective Lyapunov exponent. Since this covariant directions pointed by CLVs are not orthogonal, the sums of FTCLEs are not related to the rates of volume expansion or contraction.

In brief, FTLEs are based on backward Lyapunov vectors and are appropriate for testing volume expanding properties in tangent space. For this purpose they have to be summed, while individual values of FTLEs except the first one have no much sense. FTCLEs are based on covariant Lyapunov vectors and are good for testing the expansion or contraction of tangent vectors. Their sums have no sense and one has to consider their values individually.

The specific feature of both FTLEs and FTCLEs is that they are computed for finite-time intervals. One of the appropriate ways of employing them is analysis of their fluctuations on asymptotically large time intervals [1]. However, when local properties are required, it is usually unclear which interval $t_2 - t_1$ is sufficiently small to give a representative picture. Obviously this problem makes sense only for continuous-time systems, while for discrete-time systems the local properties are recovered by FTLEs and FTCLEs computed for unit time steps $t_2 - t_1 = 1$.

1.3. Instant Lyapunov Exponents

To analyze tangent space expansion on infinitesimal time, we will introduce here the *instant Lyapunov exponents*. Let us start with the instant Lyapunov exponents based on backward Lyapunov vectors, which will be called IBLE and denoted by $\Lambda_i(t)$. They have to be related to FTLEs $\bar{\Lambda}_i(t_1, t_2)$ as follows:

$$\bar{\Lambda}_i(t_1, t_2) = \frac{1}{t_2 - t_1} \int_{t_1}^{t_2} \Lambda_i(t)\, \mathrm{d}t. \tag{1.16}$$

On the other hand, by definition, the sum of n first FTLEs is an exponential growth rate of n-dimensional volume:

$$\sum_{i=1}^{n} \bar{\Lambda}_i(t_1, t_2) = \frac{1}{t_2 - t_1} \log \frac{\mathrm{Vol}_n(t_2)}{\mathrm{Vol}_n(t_1)}. \tag{1.17}$$

Substituting here Eq. (1.16) and differentiating by t_2, we obtain

$$\sum_{i=1}^{n} \Lambda_i(t_2) = \frac{\mathrm{d}}{\mathrm{d}t_2} \log \mathrm{Vol}_n(t_2). \tag{1.18}$$

Here we have taken into account that $\mathrm{Vol}_n(t_1)$ does not depend on t_2. Volume $\mathrm{Vol}_n(t_2)$ is equal to the product of n first diagonal elements r_{ii} of the upper triangular matrix obtained after QR decomposition, see Eq. (1.7). A detailed explanation of it can be found in [15]. Hence

$$\sum_{i=1}^{n} \Lambda_i(t_2) = \frac{\mathrm{d}}{\mathrm{d}t_2} \sum_{i=1}^{n} \log r_{ii}, \tag{1.19}$$

$$\Lambda_i(t) = \dot{r}_{ii}/r_{ii}. \tag{1.20}$$

To proceed, consider a variational equation in the matrix form:

$$\dot{\mathbf{V}} = \mathbf{J}\mathbf{V}, \tag{1.21}$$

where $\mathbf{V}$ is a matrix of tangent vectors. Substituting $\mathbf{V}$ with its QR-decomposition we obtain:

$$\dot{\mathbf{Q}}\mathbf{R} + \mathbf{Q}\dot{\mathbf{R}} = \mathbf{J}\mathbf{Q}\mathbf{R}, \tag{1.22}$$

or, after simple matrix algebra:

$$\dot{\mathbf{R}}\mathbf{R}^{-1} = \mathbf{Q}^{\mathrm{T}}\mathbf{J}\mathbf{Q} - \mathbf{Q}^{\mathrm{T}}\dot{\mathbf{Q}}. \tag{1.23}$$

For any orthogonal time-dependent matrix $\mathbf{Q}$ the product $\mathbf{Q}^{\mathrm{T}}\dot{\mathbf{Q}}$ is always skew-symmetric. It can be easily checked by differentiation of the identity $\mathbf{Q}^{\mathrm{T}}\mathbf{Q} = 1$. This means that the diagonal of $\mathbf{Q}^{\mathrm{T}}\dot{\mathbf{Q}}$ contains only zeros. Thus, substituting diagonal elements of the matrices from Eq. (1.23) into Eq. (1.20), we obtain

$$\Lambda_i(t) = q_i^{\mathrm{T}}(t)\mathbf{J}(t)q_i(t), \tag{1.24}$$

where q_i is the ith backward Lyapunov vector. Thus, to compute IBLE $\Lambda_i(t)$ in the course of usual routine for the Lyapunov exponent after steps (1.6), (1.7), we need to multiply each backward vector by the Jacobian matrix and then to find the inner product with the vector itself.

Divergence of the vector field produced by the continuous-time system (1.1) is known to be equal to the instant exponential volume contraction rate in the whole N-dimensional phase space [12]. It means that the sum of N IBLEs has to be equal to this divergence. This is indeed the case. By definition, the divergence is equal to the sum of diagonal elements of the Jacobian matrix. Thus,

$$\begin{aligned}\sum_{i=1}^{N}\Lambda_i &= \sum_{ijk} q_{ij}j_{ik}q_{kj} = \sum_{ik} j_{ik}\sum_{j} q_{ij}q_{kj} \\ &= \sum_{ik} j_{ik}\delta_{ik} = \sum_{i} j_{ii} = \operatorname{div} F,\end{aligned} \tag{1.25}$$

where q_{ij} and j_{ik} are elements of matrices $\mathbf{Q}_{\mathrm{b}}$ and $\mathbf{J}$, respectively, and δ_{ik} is Kronecker's symbol. Notice that these calculations use merely the orthogonality of $\mathbf{Q}_{\mathrm{b}}$, and do not employ its specific form. This means that this equality is rather trivial and cannot be used, for example, for testing correctness of computations of IBLEs. Also notice that a similar equality for the corresponding FTLEs can be fulfilled only approximately, since $\operatorname{div} F$ is an instant value and FTLEs are always related to a finite-time interval.

Let us now turn to the finite-time exponents based on CLVs. We will call them ICLE, denote by $\mathcal{L}_i(t)$, and introduce via the following integral:

$$\bar{\mathcal{L}}_i(t_1, t_2) = \frac{1}{t_2 - t_1}\int_{t_1}^{t_2} \mathcal{L}_i(t)\,\mathrm{d}t, \tag{1.26}$$

where $\bar{\mathcal{L}}_i(t_1, t_2)$ are FTCLE, i. e, the above-mentioned finite-time exponent based on CLVs. FTCLE is equal to the exponential growth rate of the ith CLV $\gamma_i(t)$ on the time interval $(t_2 - t_1)$[1)]:

$$\bar{\mathcal{L}}_i(t_1, t_2) = \frac{1}{t_2 - t_1}\log\left(\frac{\|\gamma_i(t_2)\|}{\|\gamma_i(t_1)\|}\right). \tag{1.27}$$

Combining Eqs. (1.26) and (1.27) and differentiating by t_2, we obtain

$$\mathcal{L}(t_2) = \frac{\mathrm{d}}{\mathrm{d}t_2}\log\|\gamma(t_2)\|. \tag{1.28}$$

[1)] Notice that using this equation for straightforward computation of FTCLE, i. e., solving the numerically variational equation with $\gamma_i(t_1)$ as an initial condition, one has to take a sufficiently short interval $t_2 - t_1$. Though formally CLVs are preserved in the course of running along a trajectory, they are fragile in the sense that any error grows. Thus the numerical approximations of CLVs slowly diverge from their true directions and tend to align along the first CLV.

Here we have taken into account that $\|\gamma(t_1)\|$ does not depend on t_2. Now we proceed as follows:

$$\begin{aligned}\mathcal{L}(t_2) &= \frac{1}{2}\frac{\mathrm{d}}{\mathrm{d}t_2}\log\|\gamma(t_2)\|^2 = \frac{1}{2\|\gamma(t_2)\|^2}\frac{\mathrm{d}}{\mathrm{d}t_2}\gamma(t_2)^{\mathrm{T}}\gamma(t_2)\\ &= \frac{1}{2\|\gamma(t_2)\|^2}\left[\dot{\gamma}(t_2)^{\mathrm{T}}\gamma(t_2) + \gamma(t_2)^{\mathrm{T}}\dot{\gamma}(t_2)\right].\end{aligned} \tag{1.29}$$

By definition, CLVs evolve according to the variational equation (1.2). Thus,

$$\mathcal{L}(t_2) = \frac{1}{2\|\gamma(t_2)\|^2}\left\{\gamma(t_2)^{\mathrm{T}}[\mathbf{J}(t_2)^{\mathrm{T}} + \mathbf{J}(t_2)]\gamma(t_2)\right\}. \tag{1.30}$$

Taking into account that CLVs are always computed with unit norms, we obtain the final equation for ICLE:

$$\mathcal{L}(t) = \frac{1}{2}\left\{\gamma(t)^{\mathrm{T}}[\mathbf{J}(t)^{\mathrm{T}} + \mathbf{J}(t)]\gamma(t)\right\}. \tag{1.31}$$

Altogether, we deal with characteristic exponents of four types. Summed FTLEs $\bar{\Lambda}_i$ and IBLEs Λ_i indicate the volume expansion occurring on finite-time intervals and instantly, respectively. FTLEs are related to IBLEs via Eq. (1.16). FTCLEs $\bar{\mathcal{L}}_i$ and ICLEs $\mathcal{L}_i$ show expansion along covariant directions on finite-time intervals and instantly, respectively. These are related to each other according to Eq. (1.26). In what follows, we will use all of them to analyze the structure of chaotic attractors.

It should be noted that, due to sensitivity to the local structure of phase space, finite-time and instant Lyapunov exponents are not invariant under variable changes in the system under consideration. However, they have topologically invariant statistical properties, for example, their first moments, i. e., the global Lyapunov exponents.

2. VERIFICATION OF PSEUDOHYPERBOLICITY

2.1. Lorenz System

We start with the famous Lorenz system [29–31]:

$$\begin{aligned}\dot{x} &= \sigma(y - x),\\ \dot{y} &= x(r - z) - y,\\ \dot{z} &= xy - bz.\end{aligned} \tag{2.1}$$

The parameters are $r = 28$, $\sigma = 10$, $b = 8/3$. To solve numerically these and other equations, we use the Runge – Kutta method of the fourth order.

First of all, we need Lyapunov exponents. For this purpose we will solve Eq. (2.1) simultaneously with its variational equations with time step $\Delta t = 10^{-4}$. Iterations (1.6), (1.7) are repeated until the maximal absolute error of λ_i becomes less than $\epsilon = 10^{-5}$. These computations are repeated ten times, and the resulting exponents are averaged. The results are $\lambda_1 = 0.906$, $\lambda_2 \approx 10^{-5}$, and $\lambda_3 = -14.573$. The second exponent must actually be put to zero since it corresponds to the symmetry of Eqs. (2.1) with respect to time shifts. The values agree well with the values reported in the literature, see, for example, [6, 32, 33].

The Lorenz system is known to be pseudohyperbolic [7, 25, 28, 34]. Our purpose here is to confirm this by testing the absence of tangencies between the volume expanding and contracting subspaces according to the property (i) formulated in the Introduction. Also, we will test how the properties (ii), (iii), and (iv) are satisfied locally.

Since $\lambda_1 + \lambda_2 > 0$ and $\lambda_3 < 0$, the tangent space of the Lorenz system (2.1) is expected to be split into two-dimensional volume expanding and one-dimensional contracting subspaces. The transversality of these two subspaces (property (i)) is confirmed by Fig. 1, where distributions of angles between tangent subspaces are shown. This and all subsequent figures have been plotted using Matplotlib graphics package [37]. Angle θ_1 is computed between the subspace related to the first covariant vector and the subspace spanned on two last ones; and θ_2 is computed between the

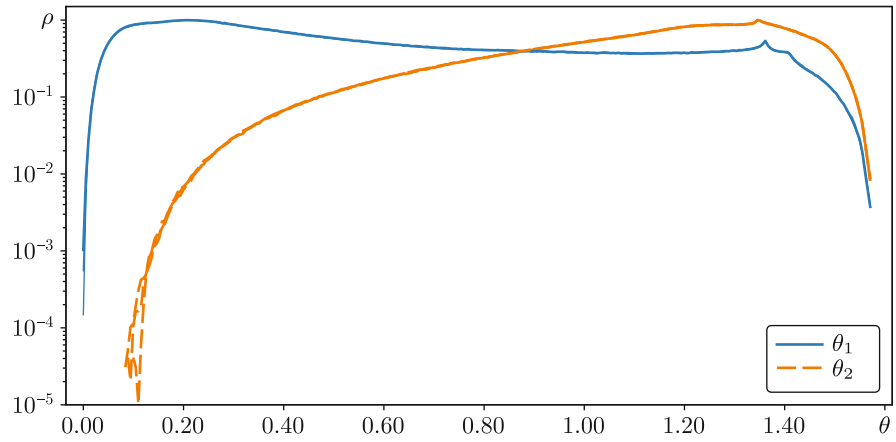

Fig. 1. Distributions of angles between tangent subspaces for the Lorenz system (2.1). Each curve is computed three times with different numerical steps $\Delta t = 0.01$, 0.001 and 0.0001. The curves coincide almost perfectly, indicating that they are not affected by time step. The pseudohyperbolicity is confirmed by the nonvanishing θ_2.

subspace of the first two covariant vectors and the last one. To check that the curves are not affected by the numerical step size, we have computed the angles three times, with steps $\Delta t = 0.01$, 0.001 and 0.0001. (For the first curve the orthogonalization and computation of the angles is done at each step, for the second one after each 10 steps and for the last one after each 100 steps.) As a result, all three curves coincide almost perfectly, so that they are barely distinguishable in the figure. One can see from the figure that the subspace of the two first vectors never has common elements with the subspace of the last one, since θ_2 never vanishes. In other words, these subspaces are hyperbolically isolated. This is the main manifestation of the pseudohyperbolicity. (Notice that the uniform hyperbolicity requires the separation of the expanding, neutral and contracting subspaces, i.e, those spanned by covariant vectors associated with positive, zero and negative Lyapunov exponents. In particular, in Fig. 1 the angle θ_1 would also be nonzero.)

Figure 2 shows the phase portrait of the Lorenz system where the attractor points are colored according to the values of θ_2: lighter colors represent larger angles and darker colors correspond to smaller ones. One can see that the large angles can be found in inner areas of the attractor, while the smallest values (but nevertheless nonzero as indicates Fig. 1) are located on its edges.

Let us now consider property (ii) concerning the volume expansion. As discussed, the volume expansion properties can be tested using Lyapunov exponents corresponding to backward Lyapunov vectors. Instant and finite-time expansion of n-dimensional volumes are characterized by n summed IBLEs Λ_i and FTLEs $\bar{\Lambda}_i$, respectively:

$$S_n(t) = \sum_{i=1}^{n} \Lambda_i(t), \quad \bar{S}_n(t, t+\tau) = \sum_{i=1}^{n} \bar{\Lambda}_i(t, t+\tau). \tag{2.2}$$

We recall that τ denotes here the averaging time.

Figure 3a shows the distributions of $S_n(t)$ and $\bar{S}_n(t, t+\Delta t)$, where Δt is a numerical discretization time step. The curves have been computed with $\Delta t = 0.01$ and 0.001, so that four curves are plotted at each n. According to Eq. (1.16), $\bar{\Lambda}_i(t, t+\Delta t) \approx \Lambda_i(t)$ if the averaging time Δt is so small that $\Lambda_i(t)$ varies slowly on the integration interval. Thus, the coincidence of the distributions for $S_n(t)$ and $\bar{S}_n(t, t+\Delta t)$ indicates that the instant exponents $\Lambda_i(t)$, though computed for a discrete subset of trajectory points, catch nevertheless all its essential features. On the other hand, $\bar{\Lambda}_i(t, t+\Delta t)$, being averaged over time step, nevertheless does not ignore essential fine details. Moreover, the coincidence of the distributions for different discretization steps Δt indicates that these results are not affected by numerical approximation errors. Altogether, the coincidence of the four distributions for each n guarantees that they are representative, i. e., adequately reveal instant volume expanding properties of the attractor.

The curve S_2 in Fig. 3 is responsible for the tested property (ii). One can see in Fig. 3a that S_2 can be both positive and negative. This means that the first subspace expanding on average due

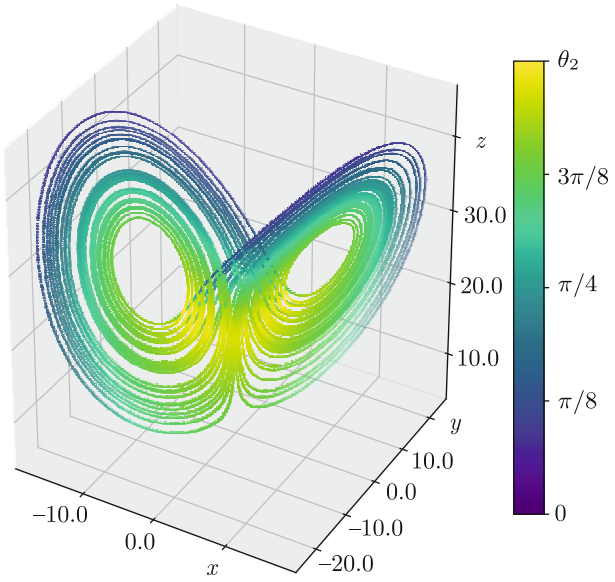

Fig. 2. Phase portrait of the Lorenz system (2.1). Point colors correspond to values of the angle θ_2 between the first two-dimensional tangent subspace and the second one-dimensional one. Observe that the small angles are located on attractor edges.

to $\lambda_1 + \lambda_2 > 0$ on infinitesimal time can be both volume expanding and contracting. Figures 3b and 3(c) show the distributions of sums of FTLEs $\bar{S}_n$ computed for finite times $\tau = 1$ and 10, respectively. Practically we average every hundred and every thousand of FTLEs, respectively, computed with the time step $\Delta t = 0.01$. One can see that only in panel (c) the distribution of $\bar{S}_2$ becomes strictly positive. Thus, the first subspace becomes expanding only on a sufficiently large time scale. Figure 4a illustrates it in more detail. It shows the behavior of the lower boundary of the distribution of $\bar{S}_2$ vs. the averaging time τ. Property (ii) is satisfied when $\min \bar{S}_2 > 0$ at roughly $\tau > 7$.

In Fig. 3 the distribution of S_3, the sum of all exponents showing the volume contraction in the whole tangent space, forms the δ peak. This contraction exponent is known to be equal to the divergence of the vector field generated by Eq. (2.1) and is equal to $-(\sigma + b + 1)$, i. e., it is constant for each trajectory. For the particular values of parameters, the divergence is $-41/3 \approx -13.67$. Analysis of the data used for plotting Fig. 3 shows that S_3 as expected is always constant and equal to this value, so that its distribution always forms the δ peak.

The verification of the property (iii) that the second subspace is contracting can be done with the help of ICLE $\mathcal{L}_n(t)$. Similar to Fig. 3a, in Fig. 5 we plot the distributions of $\mathcal{L}_n(t)$ computed with numerical steps $\Delta t = 0.01$ and 0.001 and also the distributions of the corresponding FTCLEs $\bar{\mathcal{L}}_n(t, t + \Delta t)$. The coincidence of the four curves for each exponent index n guarantees that the distributions are representative. The contraction in the second subspace is given by $\mathcal{L}_3(t)$. Observe that it is always negative, so that property (iii) is satisfied already on infinitesimal time. Figure 4b illustrates that this property is satisfied on finite times. One can see that the upper boundary of the distribution $\max \bar{\mathcal{L}}_3$ goes lower to the negative area as the averaging time τ grows.

To test if any contraction in the first subspace is exponentially weaker than the contraction in the second one (property (iv)), we consider the distribution of distances between ICLEs D_n and FTCLEs $\bar{D}_n$:

$$\begin{aligned} D_n(t) &= \min\big\{\mathcal{L}_i(t), 1 \leqslant i \leqslant n\big\} \\ &\quad - \max\big\{\mathcal{L}_i(t), n+1 \leqslant i \leqslant N\big\}, \\ \bar{D}_n(t, t+\tau) &= \min\big\{\bar{\mathcal{L}}_i(t, t+\tau), 1 \leqslant i \leqslant n\big\} \\ &\quad - \max\big\{\bar{\mathcal{L}}_i(t, t+\tau), n+1 \leqslant i \leqslant N\big\}. \end{aligned} \tag{2.3}$$

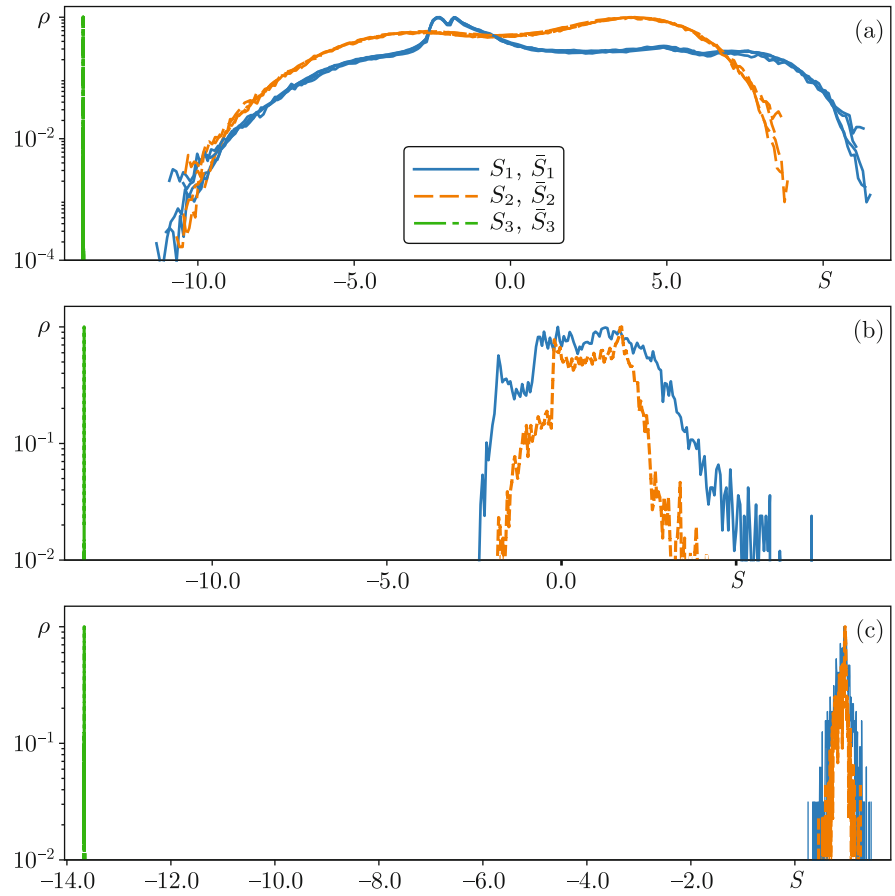

Fig. 3. Distributions of summed IBLEs and FTLEs, see Eq. (2.2), for the Lorenz system (2.1): (a) distributions of S_n and $\bar{S}_n$ computed with numerical step sizes $\Delta t = 0.01$ and 0.001 (for $\bar{S}_n$ these Δt are also used as averaging times); (b, c) distributions of $\bar{S}_n$ computed with the numerical time step $\Delta t = 0.01$ and with the averaging times $\tau = 1$ and 10, respectively. Observe that the $\bar{S}_2$ becomes strictly positive only in panel (c).

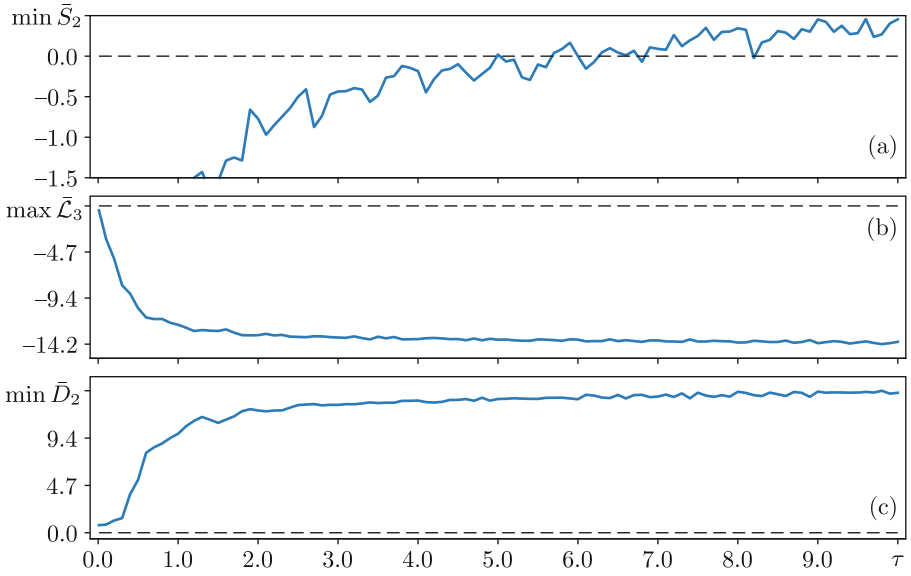

Fig. 4. Boundaries of distributions vs. averaging time τ for the Lorenz system (2.1): (a) the lower boundary of the distribution of $\bar{S}_2(t, t+\tau)$, (b) the upper boundary of $\bar{\mathcal{L}}_3(t, t+\tau)$, and (c) the lower boundary of the distribution of distances the between FTCLEs $\bar{D}_2(t, t+\tau)$. The dashed horizontal line shows zero level. Observe that $\min \bar{S}_2$ becomes positive only on a sufficiently large time scale.

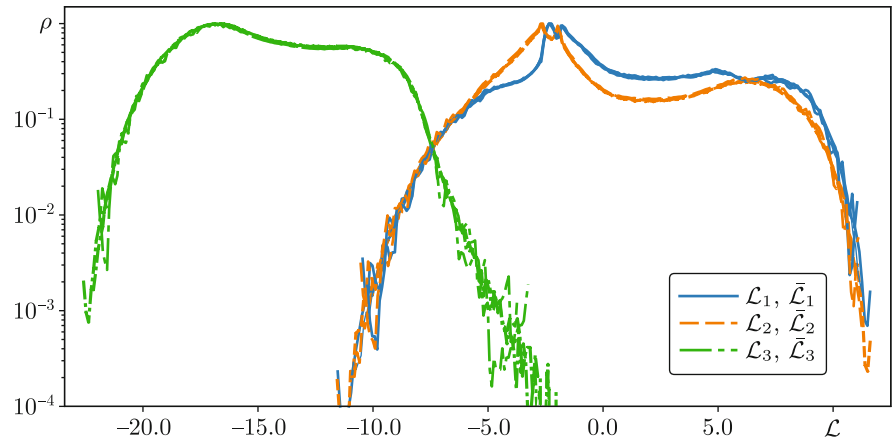

Fig. 5. Distributions of ICLEs $\mathcal{L}_i(t)$ and the corresponding finite-time exponents FTCLEs $\bar{\mathcal{L}}_i(t, t+\Delta t)$ for the Lorenz system (2.1) computed with numerical steps $\Delta t = 0.01$ and 0.001. The distribution for $\mathcal{L}_3$ is fully located on the negative semiaxis, so that the second subspace is contracting already on infinitesimal times.

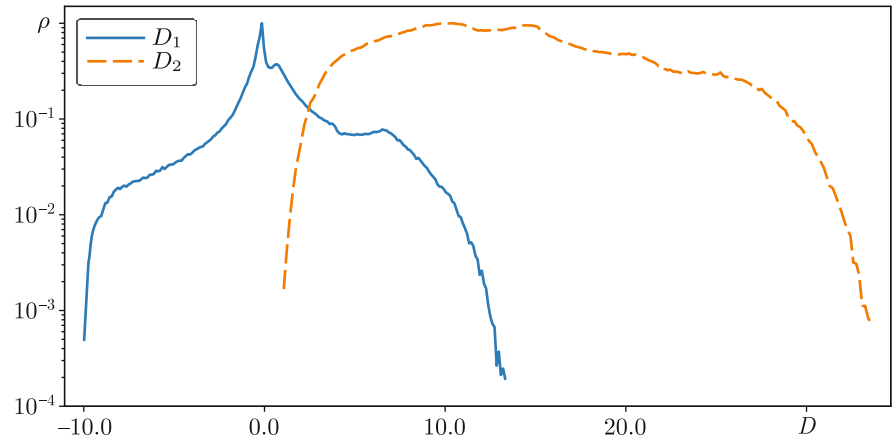

Fig. 6. Distributions of distances between ICLEs D_n, Eq. (2.3), computed with time step $\Delta t = 0.01$ for the Lorenz system (2.1). Observe that the distribution for D_2 falls onto the positive semiaxis.

This characteristic value is similar to the so-called fraction of the DOS violation criterion, which implies a pairwise comparison of FTCLEs and counting situations where $\bar{\mathcal{L}}_i < \bar{\mathcal{L}}_j$, with $j > i$. Here the abbreviation DOS stands for dominated Oseledec splitting. This characteristic value is used in [2, 4, 5] to verify the hyperbolic isolation of tangent modes in spatially distributed systems.

The splitting between the first and the second subspaces is characterized by D_2, the difference between the smallest ICLE in the first subspace $\min\{\mathcal{L}_1(t), \mathcal{L}_2(t)\}$, and ICLE from the second subspace $\mathcal{L}_3(t)$. One can see in Fig. 6 that, in agreement with property (iv), D_2 is always positive, so that any instant contraction in the first subspace is always weaker than instant contractions in the second subspace. Figure 4c shows that this property is satisfied on finite-time scales. One can see that the smallest distance $\min \bar{D}_2$ between the finite-time exponents FTCLEs goes to the positive area as averaging time τ grows.

Fluctuations around zero of D_1 in Fig. 6 indicate that inside the first subspace the first exponent $\mathcal{L}_1(t)$ can often be smaller than the second one $\mathcal{L}_2(t)$. These strong fluctuations result in the high entanglement of the corresponding covariant vectors and vanishings of the angle θ_1 in Fig. 1.

Altogether, for pseudohyperbolic Lorenz attractor we observe that the tangent space is split into two subspaces, two and one-dimensional, respectively. These subspaces are hyperbolically isolated from each other (property (i)). The second subspace is strictly contracting (property (iii)) even on infinitesimal times. If some contraction occurs in the first subspace, it is weaker than the contraction in the second subspace (property (iv)), and this property is also satisfied already on infinitesimal

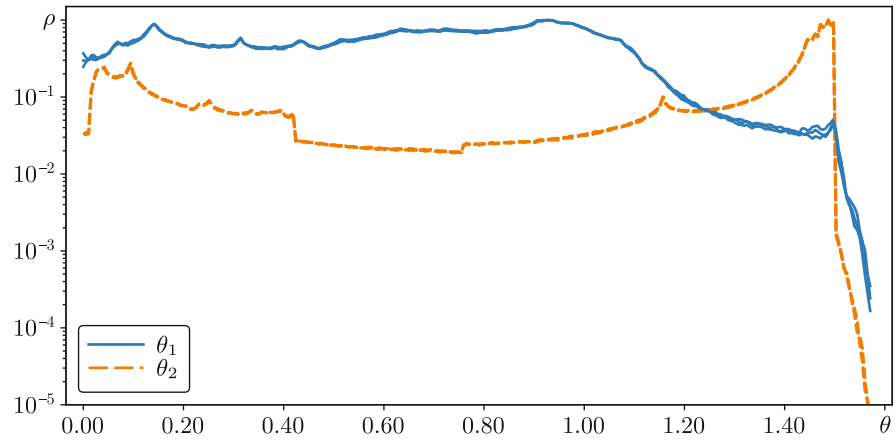

Fig. 7. Distributions of angles between tangent subspaces for the Rössler system (2.4). Each curve is computed three times with different numerical steps $\Delta t = 0.01$, 0.001 and 0.0001. Both angles often vanish, so that there are no hyperbolically isolated tangent subspaces.

time. But as for property (ii), that the first subspace always expands volumes, it is satisfied only when the volume expansion is considered on sufficiently large time scales.

2.2. Rössler System

As a counter example where the pseudohyperbolicity is absent, we consider the well-known Rössler system [31, 33, 35]

$$\begin{aligned} \dot{x} &= -y - z, \\ \dot{y} &= x + ay, \\ \dot{z} &= b + z(x - c), \end{aligned} \tag{2.4}$$

with parameters $a = 0.2$, $b = 0.2$, $c = 5.7$.

Lyapunov exponents computed with time step $\Delta t = 0.0001$ until the maximal absolute error 10^{-5} is reached and averaged over ten trajectories are $\lambda_1 = 0.072$, $\lambda_2 \approx 1 \times 10^{-6}$, and $\lambda_3 = -5.394$. The second one must be put to zero as being responsible for perturbation along the trajectory.

Though the necessary condition for pseudohyperbolicity $\lambda_1 + \lambda_2 > 0$ is fulfilled, this is not a pseudohyperbolic attractor since the first two-dimensional tangent subspace is not hyperbolically isolated from the second one-dimensional subspace: as Fig. 7 shows, the distribution for the corresponding angle θ_2 is not separated from zero. The angle θ_1 can also vanish, so that all tangent subspaces of the Rössler system are highly entangled and no splitting into hyperbolically isolated subspaces exists.

Figure 8 shows the phase portrait of the Rössler system colored according to values of the angle θ_2. One can see that the tangencies indicated by zeros of θ_2 (dark areas) occupy half the circle-like horizontal band lying parallel to the xy-plane, and also θ_2 vanishes along loops going up along the z-axis.

We have also tested related properties of the Rössler system (2.4). Figure 9 shows the distributions of summed IBLEs $S_n(t)$ and FTLEs $\bar{S}_n(t, t + \Delta t)$ indicating the volume expansion (property (ii)). As above for the Lorenz system, for each n the distributions are computed with numerical steps $\Delta t = 0.01$ and 0.001. The corresponding curves are barely distinguishable, thus confirming that they are appropriate for representation of instant expansion and contraction properties. We can see that the curves for each n have tails both in positive and negative semiaxes. They are very low for S_1 and S_2, while S_3, which is responsible for the contraction in the whole tangent space, oscillates hard. Consequently, none of the tangent subspaces is strongly contracting or expanding on infinitesimal times.

Figure 10a shows the behavior of the lower boundary of the distribution of $\bar{S}_2$, indicating the fulfillment of property (ii). One can see that $\min \bar{S}_2$ is negative and the property concerning the volume expansion remains violated even on sufficiently large time scales.

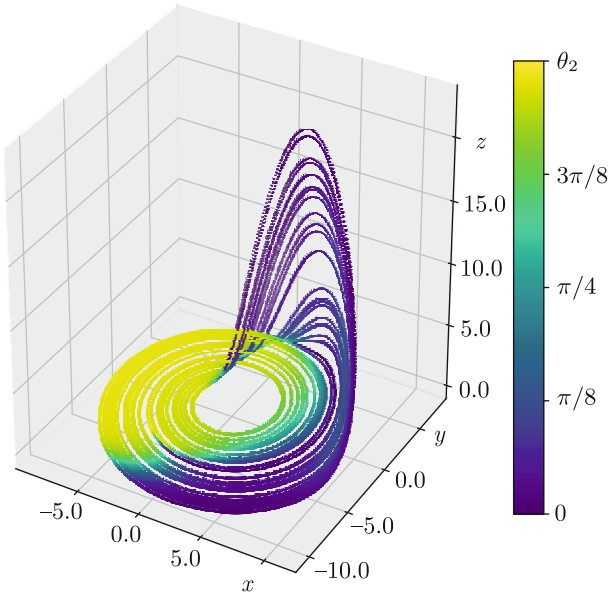

Fig. 8. Phase portrait of the Rössler system (2.4). Points are colored according to the values of θ_2. Observe a large number of points with vanishing angles.

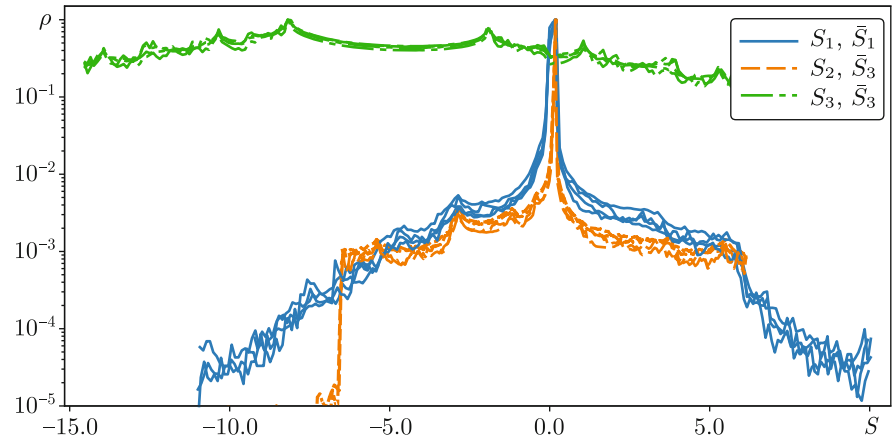

Fig. 9. Distributions of summed IBLEs and FTLEs for the Rössler system (2.4). For each n the distributions of S_n and $\bar{S}_n$ are computed with numerical step sizes $\Delta t = 0.01$ and 0.001. Observe that for all n the distributions have both positive and negative tails.

Figure 11 shows the distributions of ICLEs $\mathcal{L}_n(t)$ and the related finite-time exponents FTCLEs $\bar{\mathcal{L}}_n(t, t+\Delta t)$ to verify the contraction in the second subspace, property (iii). Again we observe that the exponents fluctuate around zero, so that any covariant direction in the tangent space on infinitesimal time can be either expanding or contracting. Nevertheless, Figure 10b shows that $\max \bar{\mathcal{L}}_3$ becomes negative at approximately $\tau > 5$, so that property (iii) is satisfied.

The distributions of distances between ICLEs (2.3) are shown in Fig. 12. The positive and negative tails of D_1 and D_2 indicate that on infinitesimal times the exponents are highly entangled and their order is not preserved. But as follows from Fig. 10c, $\min D_2$ becomes positive at finite time $\tau > 5$, so that the contraction in the second subspace becomes strictly stronger than in the first one, and property (iv) is satisfied.

So, the non-pseudohyperbolic nature of the Rössler system (2.4) is confirmed due to vanishings of angles between tangent subspaces. The strict volume expansion within the first subspace is not observed even at sufficiently large time scales. The second subspace is not strictly contracting on infinitesimal time but acquires this property on finite-time scales. The same is the case for the second subspace, which turns out to be strictly contracting on finite-time scales.

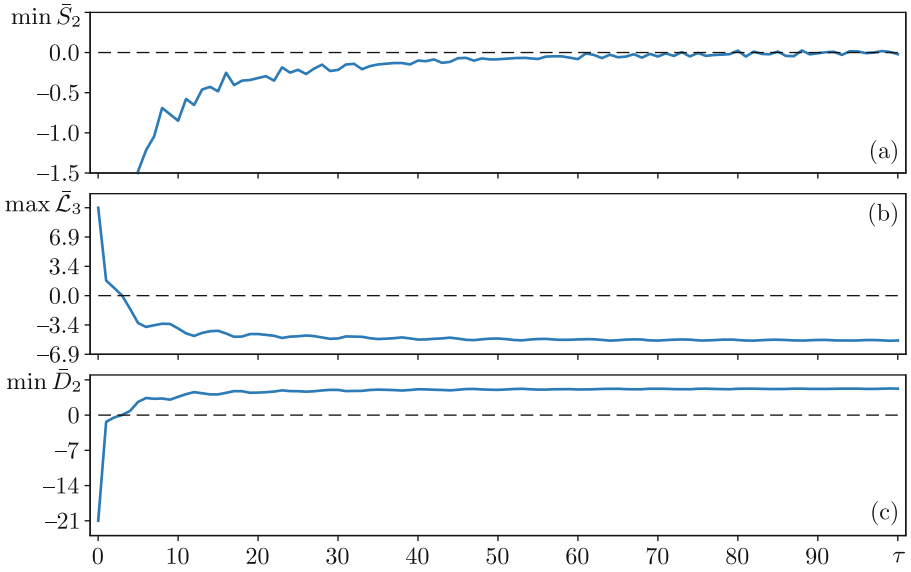

Fig. 10. As in Fig. 4 for the Rössler system (2.4).

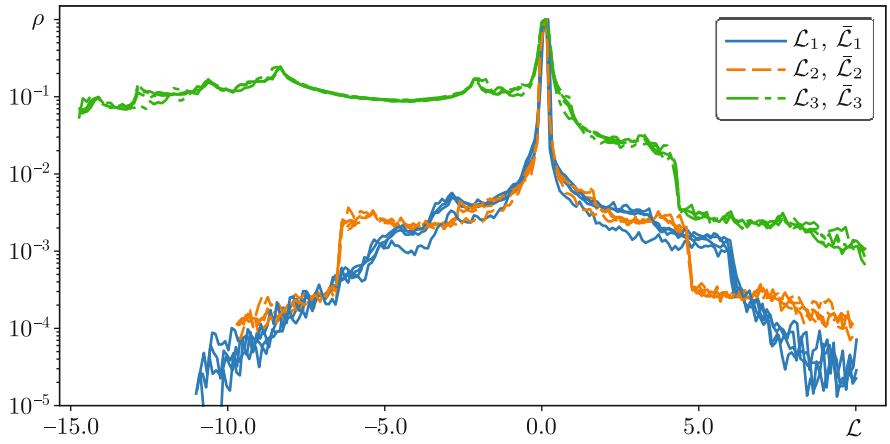

Fig. 11. Distributions of ICLEs $\mathcal{L}_i(t)$ and FTCLEs $\bar{\mathcal{L}}_i(t, t+\Delta t)$ for the Rössler system (2.4). For each index n the distributions are computed using numerical steps $\Delta t = 0.01$ and 0.001. Observe the location of all distributions both on positive and negative semiaxes.

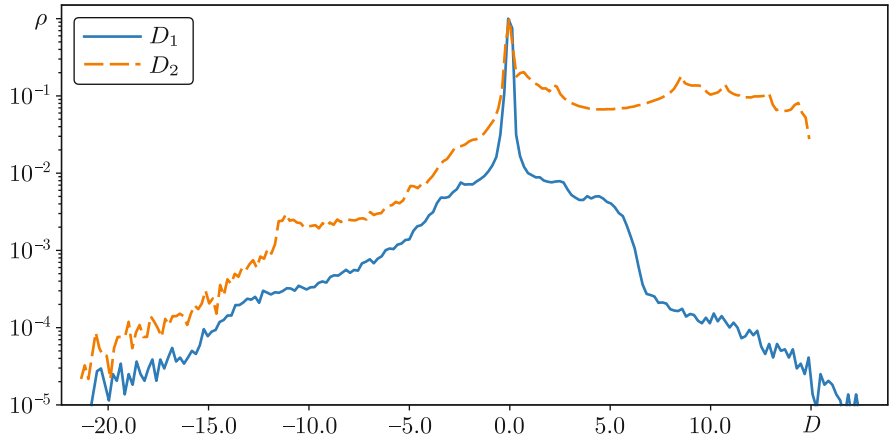

Fig. 12. Distributions of distances between ICLEs for the Rössler system (2.4) solved numerically with step size $\Delta t = 0.01$. Observe that both D_1 and D_2 can be both positive and negative.

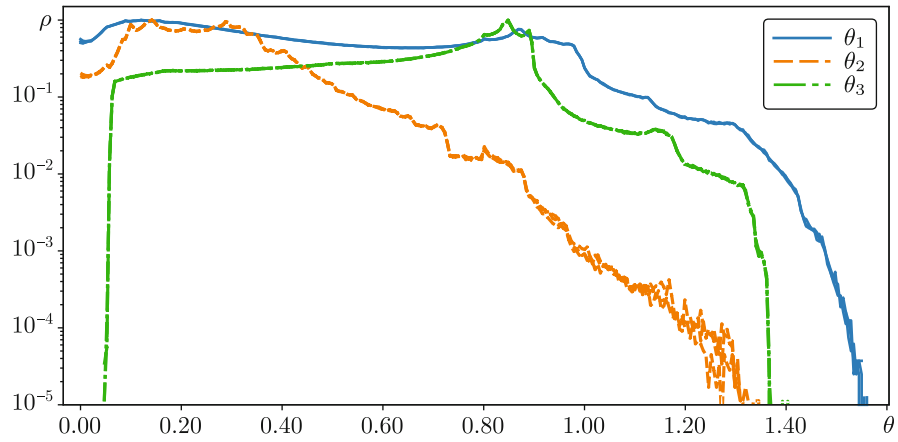

Fig. 13. Distributions of angles between tangent subspaces for the system (2.5). Each curve is computed three times with different numerical steps $\Delta t = 0.01$, 0.001 and 0.0001. The pseudohyperbolicity is indicated by the distribution of θ_3 that is well detached from the origin.

2.3. Generalized Lorenz System

Now we will analyze a generalization of the Lorenz system proposed in [40], see problem C.7.No.86, as a possible candidate for a system with a wild spiral attractor. Also, this system, as well as other examples of spiral chaos, is considered in [24, 41, 42].

$$\begin{aligned} \dot{x} &= \sigma(y - x), \\ \dot{y} &= x(r - z) - y, \\ \dot{z} &= xy - bz + \mu w, \\ \dot{w} &= -bw - \mu z, \end{aligned} \tag{2.5}$$

where parameters are $r = 25$, $\sigma = 10$, $b = 8/3$, and $\mu = 7$.

Theoretical evaluations suggest that this system is pseudohyperbolic. Lyapunov exponents computed similarly to the two previous systems are $\lambda_1 = 2.193$, $\lambda_2 = 0$, $\lambda_3 = -1.959$, and $\lambda_4 = -16.567$. Since $\lambda_1 + \lambda_2 + \lambda_3 > 0$ and $\lambda_4 < 0$, the tangent space splitting responsible for the pseudohyperbolicity, see property (i), is expected to occur between three-dimensional volume expanding first subspace and one-dimensional contracting second subspace. Figure 13 shows the distributions of angles between the tangent subspaces. The splitting of interest is characterized by the angle θ_3. Clear separation of its distribution from the origin confirms that the first and the second subspaces are hyperbolically isolated, so that the system (2.5) is indeed pseudohyperbolic. Notice also high frequency of vanishing of θ_1 and θ_2 indicating that within the first subspace the trajectory manifolds spanned by the corresponding first three CLVs are highly entangled.

Figure 14 shows how values of θ_3 are located on the attractor of the system (2.5). It represents a three-dimensional projection of the attractor whose points are colored according to values of θ_3. Observe that both the projection itself and the distribution of angles on it is similar to the Lorenz attractor: it contains two circular bands where small angles are located on outer edges, cf. Fig. 2.

Figure 15 provides verification of the volume expansion, property (ii), demonstrating the distributions of summed exponents S_n and $\bar{S}_n$. As for the previous systems, each curve is computed four times: for IBLEs and FTLEs with numerical steps $\Delta t = 0.01$ and 0.001. The almost perfect coincidence of the different versions of the curves confirms that they are representative for characterizing the properties of the attractor on infinitesimal times.

The volume expansion within the first subspaces is shown by the distribution for S_3. One can see that it hardly oscillates, being with almost equal probabilities both positive and negative. This means that the property (ii) does not hold on infinitesimal time. To check when this property is satisfied in Fig. 16, we have plotted the lower boundary of the distribution $\min \bar{S}_3$ vs. averaging time τ. One can see that $\min \bar{S}_3 > 0$ at approximately $\tau > 7$. This means that the first tangent subspace of the system (2.5) becomes volume expanding at sufficiently large time scales.

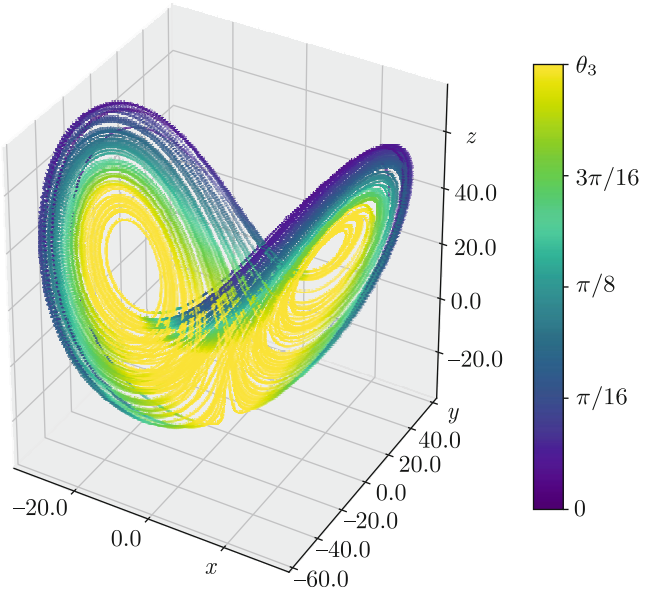

Fig. 14. Attractor for the system (2.5). Colors correspond to values of θ_3. Observe similarity with the Lorenz attractor in Fig. 2.

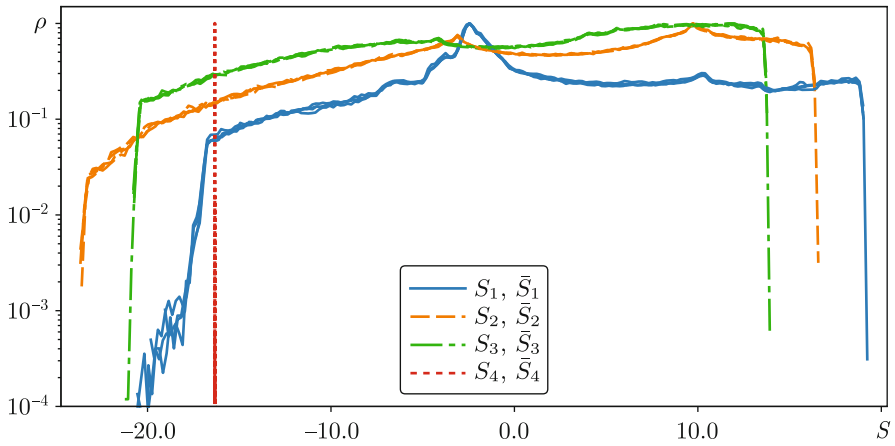

Fig. 15. Distributions of summed IBLE S_n and FTLEs $\bar{S}_n$ for the system (2.5) computed with numerical steps $\Delta t = 0.01$ and 0.001. Observe that S_3 can have both positive and negative signs.

In Fig. 15 one can see that the distribution for S_4, similarly to the Lorenz system, forms the δ peak, cf. distribution for S_3 in Fig. 3a. One can check that this is due to the constant divergence $\operatorname{div} F = -(\sigma + 2b + 1)$, which for the given parameter values is equal to -16.3.

Property (iii) concerning the strong contraction in the second subspace is tested in Fig. 17. Again each distribution is represented with four curves: ICLEs and FTCLEs are computed with numerical time steps $\Delta t = 0.01$ and 0.001. One can see that $\mathcal{L}_4(t)$ responsible for contraction in the second subspace, though rarely, can be positive. Therefore, on infinitesimal time the property (iii) does not hold. As one can see in Fig. 16b, the upper boundary of the distribution $\max \bar{\mathcal{L}}_4$ becomes negative at approximately $\tau > 1$, and the second subspace becomes strongly contracting on finite-time scales.

According to property (iv), any contraction in the first subspace is weaker than contraction in the second subspace. This is tested using distributions of distances between exponents D_n in Fig. 18. The splitting between the first and the second tangent subspaces is characterized by D_3. One can see that D_3 can rarely be negative. This means that sometimes instant contraction in the first subspace is stronger than that in the second subspace, and property (iv) does not hold

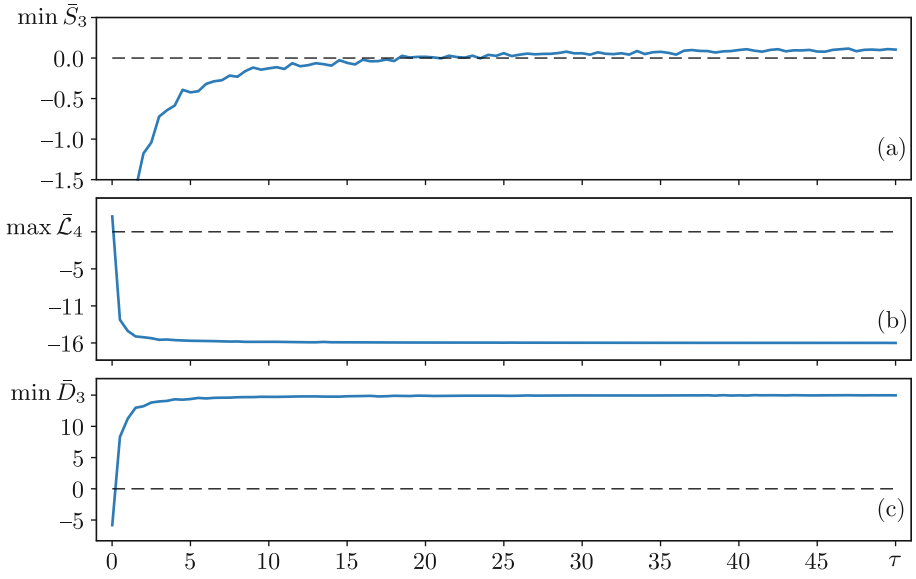

Fig. 16. As in Fig. 4 for the system (2.5).

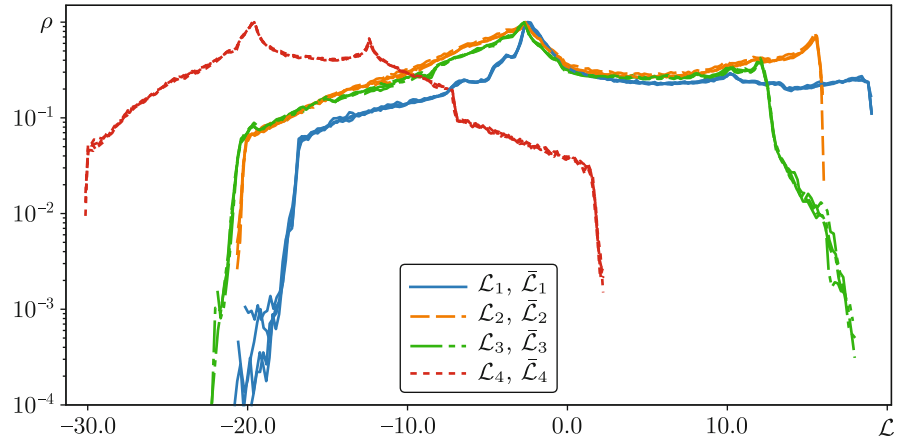

Fig. 17. (a) Distributions of ICLEs and FTCLEs computed with time steps $\Delta t = 0.01$ and 0.001 for the system (2.5). Observe that $\mathcal{L}_4$ can be both positive and negative.

on infinitesimal times. As follows from Fig. 16c, the lower boundary $\min \bar{D}_3$ becomes positive at approximately $\tau > 1$, so that property (iv) is satisfied on finite-time scales.

Altogether, for the generalized Lorenz system (2.5), the pseudohyperbolicity is confirmed due to the absence of tangencies between the first three-dimensional subspace and the second one-dimensional subspace, property (i). But all other properties are satisfied only on finite-time scales, and are violated on infinitesimal times. Volumes from the first subspace can instantly be contracting, and vectors from the second one can sometimes be expanded. Moreover, the instant contraction in the first subspace can sometimes be stronger than the contraction in the second subspace.

2.4. Three-Dimensional Generalizations of Hénon Map

A series of works have recently been reported where a pseudohyperbolicity of three-dimensional generalizations of the Hénon map are discussed [8, 24, 28, 36]. In this paper we will test the pseudohyperbolicity of the map

$$\begin{aligned} x_{n+1} &= y_n, \\ y_{n+1} &= z_n, \\ z_{n+1} &= Bx_n + Az_n + Cy_n - z_n^2, \end{aligned} \tag{2.6}$$

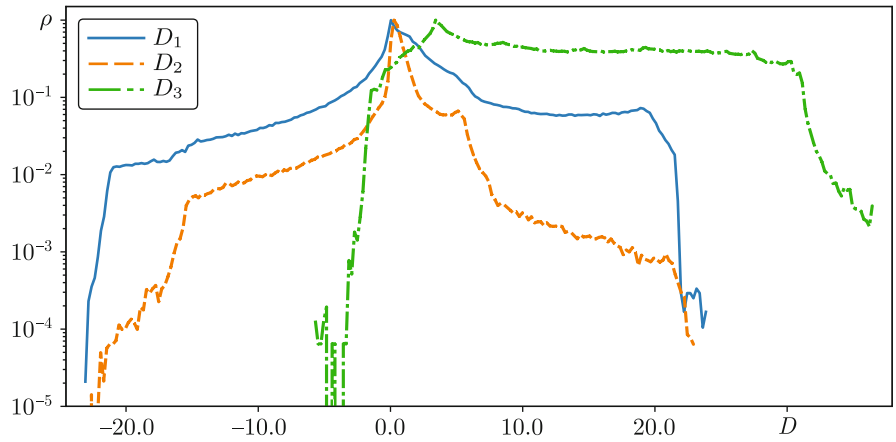

Fig. 18. Distributions of distances between ICLEs for the system (2.5). Numerical step size is $\Delta t = 0.01$. Observe that D_3 changes sign.

with following parameter sets

$$B = 0.7,\ A = -1.11,\ C = 0.77, \tag{2.7}$$

$$B = 0.7,\ A = 0,\ C = 0.85, \tag{2.8}$$

$$B = 0.7,\ A = 0,\ C = 0.815. \tag{2.9}$$

Parameters (2.7) correspond to Eq. (17) and Fig. 5d in [8], and parameters (2.8) and (2.9) are taken from [36], see Eq. (1) and Fig. 1 there.

As reported in [24], mathematicians from the University of Uppsala, Sweden, J. Figueros and W. Tucker using the interval arithmetic methods have not confirmed the pseudohyperbolicity of the system (2.6) with parameters (2.8) and confirmed it for the parameters (2.9).

Lyapunov exponents computed with maximal absolute error $\epsilon = 10^{-5}$ and averaged over ten independent trajectories are the following: for (2.7) $\lambda_1 = 0.013$, $\lambda_2 = 0$, $\lambda_3 = -0.370$; for (2.8) $\lambda_1 = 0.020$, $\lambda_2 = 0$, $\lambda_3 = -0.377$; and for (2.9) $\lambda_1 = 0.008$, $\lambda_2 = 0$, $\lambda_3 = -0.365$. Notice that the second Lyapunov exponent is always zero. As discussed in Ref. [43, 44], each zero exponent is related with a continuous symmetry of a system. As one can check, the system (2.6) is invariant under the transformation $x_n \to y_n C/B$ and $y_n \to x_n B/C$. In tangent space this transformation gives rise to a direction with marginal stability, which, in turn, results in zero Lyapunov exponent.

The presence of the pseudohyperbolicity is tested in Fig. 19, where the distributions of angles between tangent subspaces are shown, property (i). Since for all cases $\lambda_1 + \lambda_2 > 0$ and $\lambda_3 < 0$, the first subspace is two-dimensional and the second is one-dimensional. This means that the angle θ_2 indicates the presence or absence of the pseudohyperbolicity. As one can see in Fig. 19a and 19c, the nonvanishing θ_2 indicates that parameters (2.7) and (2.9) correspond to a pseudohyperbolic attractor, i. e., property (i) is satisfied. On the contrary, in Fig. 19b the distribution for θ_2 is not separated from the origin, i. e., the first and the second subspaces are not hyperbolically isolated, so that the case (2.8) is not pseudohyperbolic.

Phase portraits of the system (2.6) with parameters (2.7)–(2.9) are shown in Figs. 20–22, respectively. Colors represent values of the angle θ_2. Observe high similarity of the pseudohyperbolic attractors in Figs. 20 and 22. Their small (but nonzero) angles θ_2 are located on bands crossing in the center of the attractor. On the non-pseudohyperbolic attractor in Fig. 21 small and zero angles are located on edge areas.

The instant exponents IBLEs and ICLEs are not applicable to discrete-time systems like (2.6) since the local expansions and contractions are explored by FTLEs and FTCLEs computed for one step of time. Hence, we will consider only finite-time exponents. Moreover, the distributions of $\bar{S}_n$, $\bar{\mathcal{L}}_n$, and $\bar{D}_n$ will be represented only for the parameters (2.7) since two other cases produce similar pictures.

Figure 23 shows that for the case (2.7) property (ii) is locally violated and the first subspace is not strictly volume expanding. The indication is that $\bar{S}_2$ oscillates, being often positive

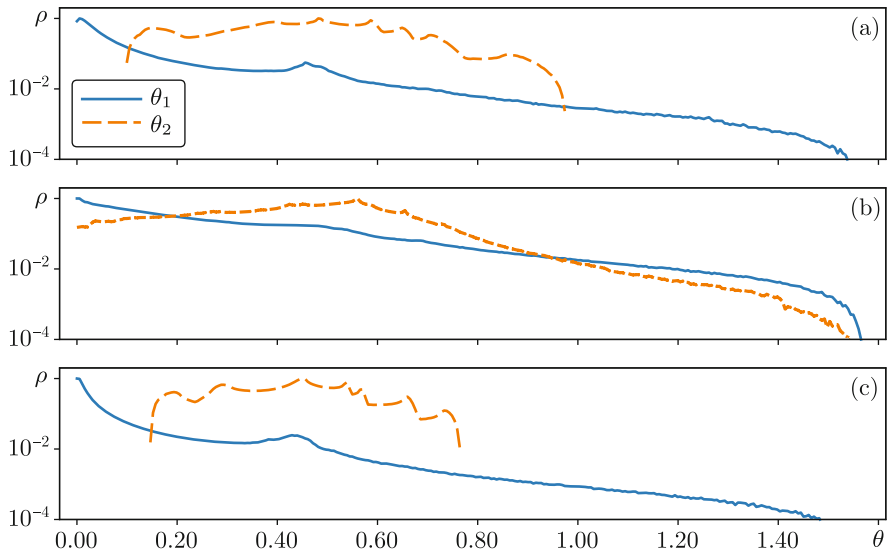

Fig. 19. Distributions of angles between tangent subspaces for the system (2.6). Panels (a), (b), and (c) correspond to parameters (2.7)–(2.9). The nonvanishing θ_2 confirms the pseudohyperbolicity in panels (a) and (c), while the case represented in panel (b) is not pseudohyperbolic.

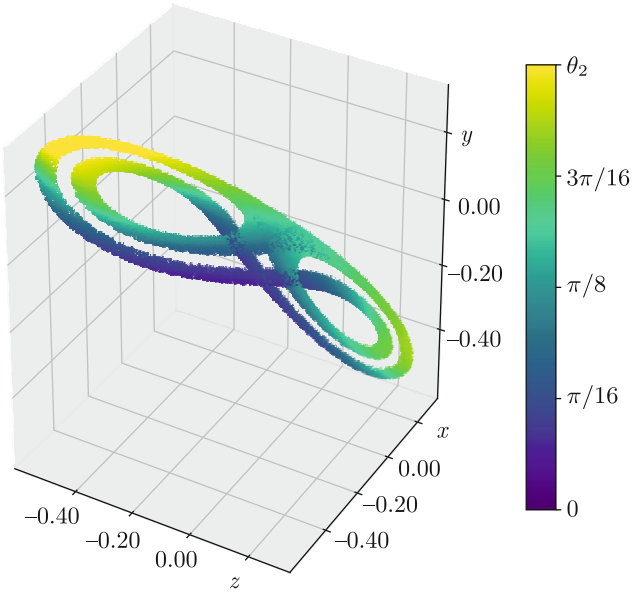

Fig. 20. Attractor of the system (2.6) with parameters (2.7). Colors represent values of θ_2. Observe the location of small angles in the middle area.

and negative. Analogously, $\bar{S}_2$ oscillates for the cases (2.8) and (2.9), so that property (ii) is also not satisfied locally. As one can see in Fig. 24a, the lower boundary of the distribution $\min \bar{S}_2$ becomes positive only on sufficiently large time scales in all the three cases considered. Observe almost identical behavior of $\min \bar{S}_2$ for pseudohyperbolic attractors, see curves 1 and 3 corresponding to parameters (2.7) and (2.9), respectively. For the non-pseudohyperbolic attractor with parameters (2.8) the first subspace also becomes strictly expanding, i. e., $\min \bar{S}_2$ becomes positive, but on a much higher time scale. As for the distribution for $\bar{S}_3$ in Fig. 23, δ peak indicates that the contraction in the whole tangent space of the system (2.6) is constant.

Figure 25 demonstrates a local violation of property (iii) for the parameters (2.7): $\bar{\mathcal{L}}_3$ responsible for the contraction in the second subspace can sometimes be positive. Also, $\bar{\mathcal{L}}_3$ demonstrates similar behavior for parameter (2.8) and (2.9). Figure 24b shows that the second subspace for all three

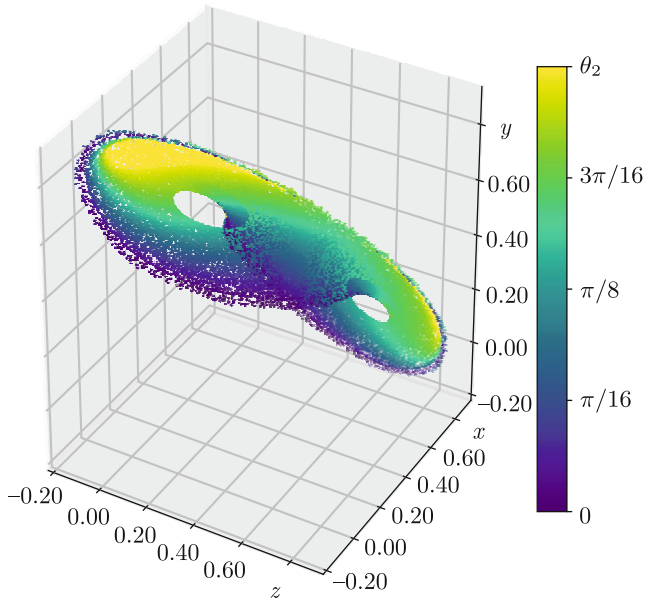

Fig. 21. Attractor of the system (2.6), (2.8). Observe vanishing angles on the edges.

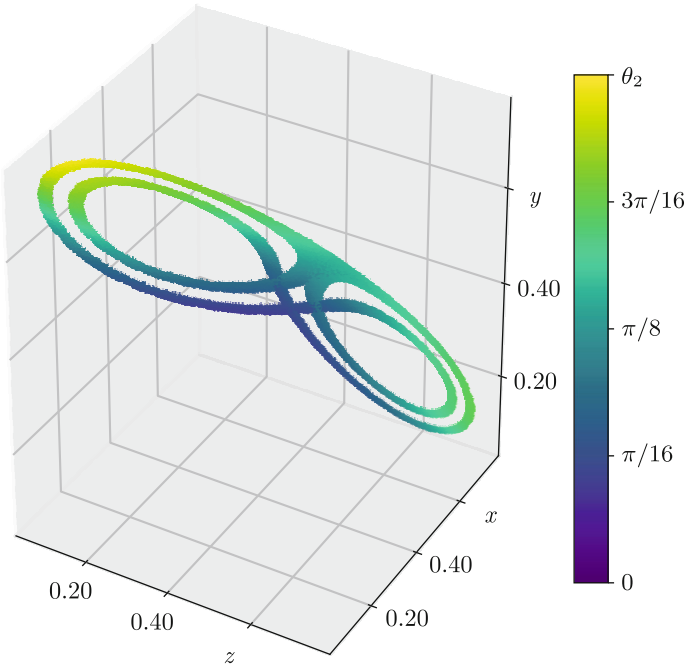

Fig. 22. Attractor of the system (2.6), (2.9). Observe similarity with the attractor in Fig. 20.

parameter sets becomes contracting when averaging time τ grows. Again two pseudohyperbolic cases (2.7), and (2.9), curves 1 and 3, respectively, behave almost identically, and the non-pseudohyperbolic attractor with parameters (2.8), curve 2, becomes contracting much later than the other two.

Finally, property (iv) is also satisfied only on average, i. e., contraction in the first subspace can locally be stronger than contraction in the second one. One can see in Fig. 26 that indicating it $\bar{D}_2$ appears both in positive and in negative semiaxes. Similarly, $\bar{D}_2$ behaves for the cases (2.8) and (2.9). Only at approximately $\tau > 10$ min $\bar{D}_2$ becomes positive for all three cases, see Fig. 24c.

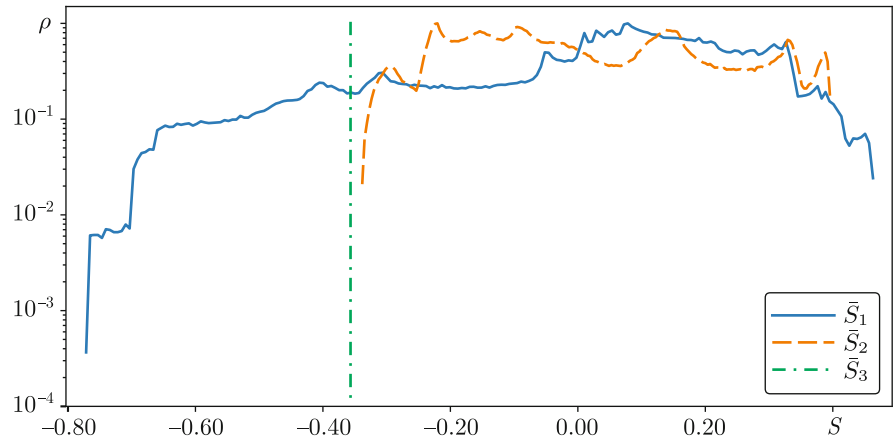

Fig. 23. Distributions of summed FTLEs $\bar{S}_n(t, t+1)$ for the system (2.6) with parameters (2.7). Observe that all three fluctuating values can change signs.

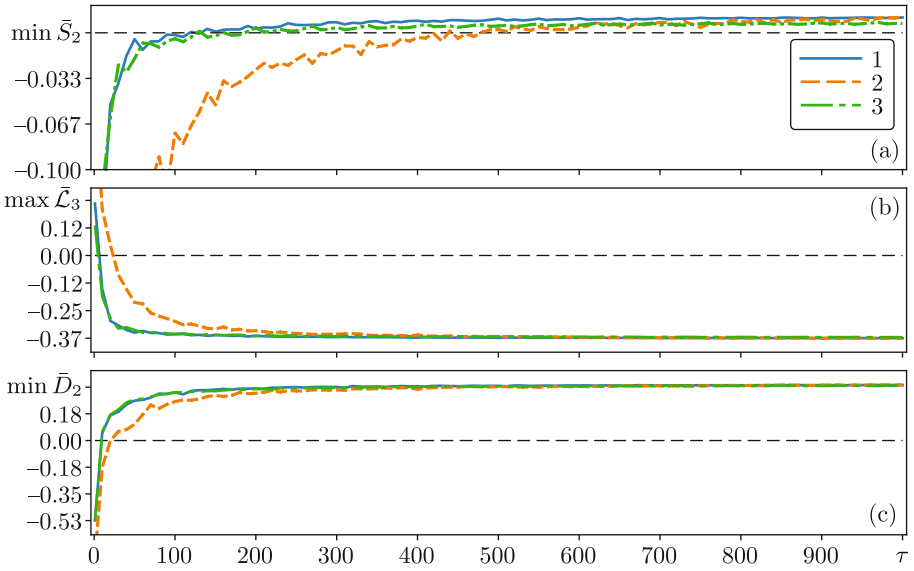

Fig. 24. As in Fig. 4 for the system (2.6) with parameters (2.7)–(2.9), respectively, curves 1, 2, and 3. Observe almost perfect coincidence of the curves 1 and 3 corresponding to the pseudohyperbolic cases.

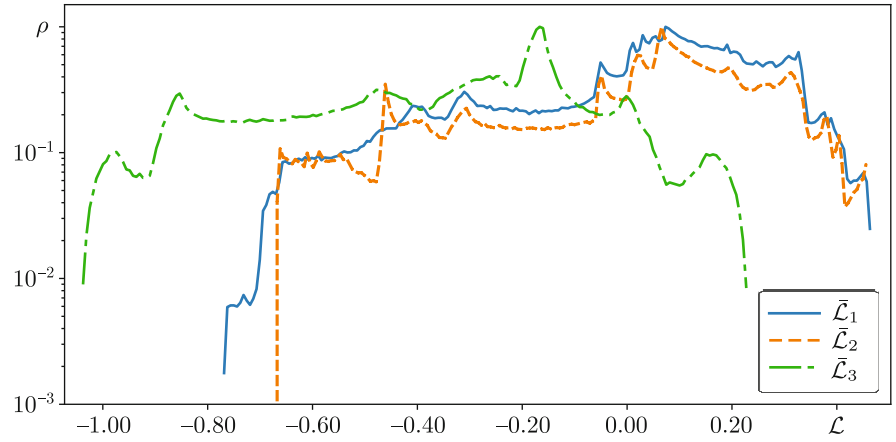

Fig. 25. Distributions of FTCLEs $\bar{\mathcal{L}}_n(t, t+1)$ for the system (2.6) with parameters (2.7). Observe that all three FTCLE can be both positive and negative.

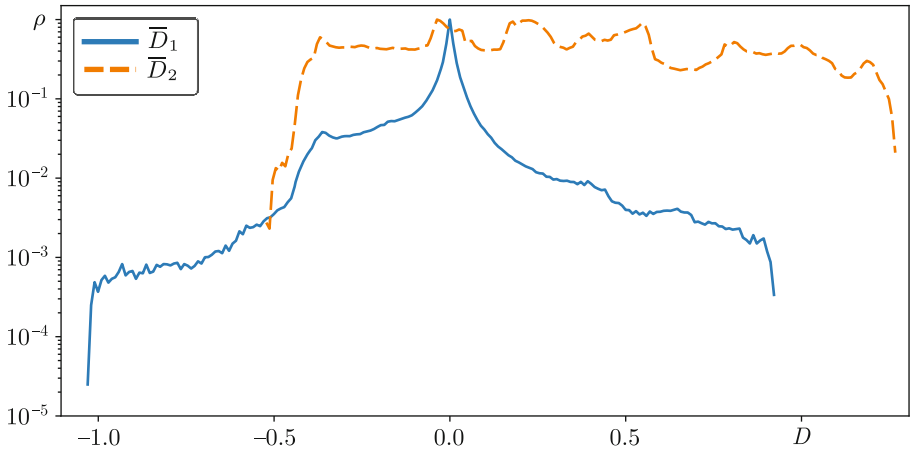

Fig. 26. Distributions of distances between FTCLEs $\bar{D}_n(t, t+1)$ for the system (2.6) with parameters (2.7). Observe that two represented values oscillate around zero.

Again notice the coincidence of the curves 1 and 3, representing pseudohyperbolic cases (2.7) and (2.9), respectively.

Altogether, the pseudohyperbolicity of the system (2.6) with parameters (2.7) and (2.9) is confirmed by the fulfillment of property (i), i. e., by the nonvanishing angle between the first two-dimensional subspace and the second one-dimensional one. In agreement with above-mentioned results, the case (2.8) is not pseudohyperbolic. The three other properties (ii), (iii) and (iv) are violated locally. They are satisfied only after averaging on a certain time scale.

3. CONCLUSION

We have tested the local structure of chaotic attractors related to pseudohyperbolicity. The classical Lorenz system has been discussed as a well-known representative of pseudohyperbolic systems, and the Rössler system has been compared with it as an example of a system not belonging to this category. Moreover, several recently reported examples [8, 24, 36] of systems with and without pseudohyperbolicity have been analyzed.

The main criterion of the pseudohyperbolicity is the splitting of the tangent space into two hyperbolically isolated subspaces, volume expanding and contracting ones. This means that the angles between these two subspaces are nonzero at every point of the attractor. We have computed numerically the corresponding angle distributions and discussed the presence or absence of the pseudohyperbolicity in the systems considered.

The properties of the two tangent subspaces of pseudohyperbolic systems are usually explored via Lyapunov exponents λ_i. The first n-dimensional subspace of a pseudohyperbolic system has to be volume expanding, so that $\sum_{i=1}^{n} \lambda_i > 0$, and the second subspace is contracting, i.e., $\lambda_i < 0$ for $i > n$. Moreover, as discussed in [8, 25, 27, 28], a contraction, if it occurs in the first subspace, has to be weaker than any contraction in the second subspace. However, Lyapunov exponents describe attractors globally and the local properties are not taken into account. Therefore, we have analyzed local, i. e., related to infinitesimal and short time intervals, volume expanding and contracting properties of the two tangent subspaces.

To analyze expansion in tangent space on infinitesimal time, we have introduced a family of instant Lyapunov exponents. Unlike the well-known finite-time ones, the instant Lyapunov exponents show expansion or contraction on infinitesimal time intervals. Two types of instant Lyapunov exponents are defined. One is related to ordinary finite-time Lyapunov exponents (FTLEs) computed in the course of standard algorithm for Lyapunov exponents. These instant exponents are based on orthogonal Gram – Schmidt vectors, also known as backward Lyapunov vectors, and we refer to them as IBLE. Their sums reveal volume expanding properties: the sum of the first n IBLEs is the exponent of growth or contraction of an n-dimensional tangent volume on infinitesimal time. The other type of instant Lyapunov exponents shows how covariant Lyapunov vectors grow or decay on infinitesimal time and thus are called ICLE. They are appropriate for analysis of instant single expanding or contraction direction in the tangent space.

Using both instant and finite-time Lyapunov exponents, we have demonstrated that for the Lorenz system the second subspace is contracting on infinitesimal times and any instant contraction in the first subspaces is always weaker than the contraction in the second one. But the first subspace is not strictly volume expanding when considered on infinitesimal times. This property is satisfied only when the volumes evolution is observed on sufficiently large finite-time scales. For other tested systems all expanding and contracting properties specific to the pseudohyperbolicity are observed only on finite times. Instantly volumes from the first subspace can sometimes be contracting, directions in the second subspace can sometimes be expanded, and the instant contraction in the first subspace can sometimes be stronger than the contraction in the second subspace.

ACKNOWLEDGMENTS

The work of SPK on theoretical formulations was supported by the Russian Science Foundation under grant No 15-12-20035. The work of PVK on elaborating computer routines and numerical computations was supported by RFBR under grant No 16-02-00135.

REFERENCES

1. Kuptsov, P. V. and Politi, A., Large-Deviation Approach to Space-Time Chaos, *Phys. Rev. Lett.,* 2011, vol. 107, no. 11, 114101, 5 pp.
2. Kuptsov, P. V. and Parlitz, U., Strict and Fussy Mode Splitting in the Tangent Space of the Ginzburg – Landau Equation, *Phys. Rev. E,* 2010, vol. 81, no. 3, 036214, 6 pp.
3. Kuptsov, P. V. and Kuznetsov, S. P., Numerical Test for Hyperbolicity in Chaotic Systems with Multiple Time Delays, *Commun. Nonlinear Sci. Numer. Simul.,* 2018, vol. 56, Suppl. C, pp. 227–239.
4. Yang, H. L., Takeuchi, K. A., Ginelli, F., Chaté, H., and Radons, G., Hyperbolicity and the Effective Dimension of Spatially Extended Dissipative Systems, *Phys. Rev. Lett.,* 2009, vol. 102, no. 7, 074102, 4 pp.
5. Takeuchi, K. A., Yang, H. L., Ginelli, F., Radons, G., and Chaté, H., Hyperbolic Decoupling of Tangent Space and Effective Dimension of Dissipative Systems, *Phys. Rev. E,* 2011, vol. 84, no. 4, 046214, 19 pp.
6. Sprott, J. C., *Elegant Chaos: Algebraically Simple Chaotic Flows,* Singapore: World Sci., 2010.
7. Bonatti, Ch., Díaz, L. J., and Viana, M., *Dynamics beyond Uniform Hyperbolicity: A Global Geometric and Probabilistic Perspective,* Encyclopaedia Math. Sci., vol. 102, Berlin: Springer-Verlag, 2005.
8. Gonchenko, A. S. and Gonchenko, S. V., Variety of Strange Pseudohyperbolic Attractors in Three-Dimensional Generalized Hénon Maps, *Phys. D,* 2016, vol. 337, pp. 43–57.
9. Benettin, G., Galgani, L., Giorgilli, A., and Strelcyn, J.-M., Lyapunov Characteristic Exponents for Smooth Dynamical Systems and for Hamiltonian Systems: A Method for Computing All of Them: P. 1: Theory, *Meccanica,* 1980, vol. 15, no. 1, pp. 9–20.
10. Ginelli, F., Poggi, P., Turchi, A., Chaté, H., Livi, R., and Politi, A., Characterizing Dynamics with Covariant Lyapunov Vectors, *Phys. Rev. Lett.,* 2007, vol. 99, no. 13, 130601, 4 pp.
11. Golub, G. H. and Van Loan, Ch. F., *Matrix Computations,* 4th ed., Baltimore, Md.: Johns Hopkins Univ., 2013.
12. Katok, A. and Hasselblatt, B., *Introduction to the Modern Theory of Dynamical Systems,* Encyclopedia Math. Appl., vol. 54, Cambridge: Cambridge Univ. Press, 1995.
13. Kuptsov, P. V., Fast Numerical Test of Hyperbolic Chaos, *Phys. Rev. E,* 2012, vol. 85, no. 1, 015203(R), 4 pp.
14. Kuptsov, P. V. and Kuznetsov, S. P., Numerical Test for Hyperbolicity of Chaotic Dynamics in Time-Delay Systems, *Phys. Rev. E,* 2016, vol. 94, no. 1, 010201(R), 7 pp.
15. Kuptsov, P. V. and Parlitz, U., Theory and Computation of Covariant Lyapunov Vectors, *J. Nonlinear Sci.,* 2012, vol. 22, no. 5, pp. 727–762.
16. Kuznetsov, S. P., *Hyperbolic Chaos: A Physicist's View,* Berlin: Springer, 2012.
17. Kuznetsov, S. P., Dynamical Chaos and Uniformly Hyperbolic Attractors: From Mathematics to Physics, *Phys. Uspekhi,* 2011, vol. 54, no. 2, pp. 119–144; see also: *Uspekhi Fiz. Nauk,* 2011, vol. 181, no. 2, pp. 121–149.
18. Legras, B. and Vautard, R., A Guide to Lyapunov Vectors, in *Proc. ECMWF Seminar on Predictability (Shinfield Park, Reading, UK, Sept 4–8, 1995): Vol. 1,* T. Palmer (Ed.), Reading, UK: ECMWF, 1996, pp. 143–156.
19. Shimada, I. and Nagashima, T., A Numerical Approach to Ergodic Problem of Dissipative Dynamical Systems, *Progr. Theoret. Phys.,* 1979, vol. 61, no. 6, pp. 1605–1616.
20. Hogben, L., *Handbook of Linear Algebra,* 2nd ed., Boca Raton, Fla.: CRC, 2017.
21. Pesin, Ya. B., *Lectures on Partial Hyperbolicity and Stable Ergodicity,* Zur. Lect. Adv. Math., Zürich: EMS, 2004.

22. Pikovsky, A. and Politi, A., *Lyapunov Exponents: A Tool to Explore Complex Dynamics,* Cambridge: Cambridge Univ. Press, 2016.
23. Wolfe, Ch. L. and Samelson, R. M., An Efficient Method for Recovering Lyapunov Vectors from Singular Vectors, *Tellus A,* 2007, vol. 59, no. 3, pp. 355–366.
24. Gonchenko, S. V., Gonchenko, A. S., Kazakov, A. O., and Kozlov, A. D., Elements of Contemporary Mathematical Theory of Dynamical Chaos: Part 1. Pseudohyperbolic Attractors, arXiv:1712.04032 (2017).
25. Turaev, D. V. and Shil'nikov, L. P., An Example of a Wild Strange Attractor, *Sb. Math.,* 1998, vol. 189, nos. 1–2, pp. 291–314; see also: *Mat. Sb.,* 1998, vol. 189, no. 2, pp. 137–160.
26. Dmitriev, A. S., Efremova, E. V., Maksimov, N. A., and Panas, A. I., *Generation of Chaos*, Moscow: Tekhnosfera, 2012 (Russian).
27. Turaev, D. V. and Shil'nikov, L. P., Pseudohyperbolicity and the Problem of the Periodic Perturbation of Lorenz-Type Attractors, *Dokl. Math.,* 2008, vol. 77, no. 1, pp. 17–21; see also: *Dokl. Akad. Nauk,* 2008, vol. 418, no. 1, pp. 23–27.
28. Gonchenko, A. S., Gonchenko, S. V., Kazakov, A. O., and Kozlov, A. D., Mathematical Theory of Dynamical Chaos and Its Applications: Review. Part 1. Pseudohyperbolic Attractors, *Izv. Vyssh. Uchebn. Zaved. Prikl. Nelin. Dinam.,* 2017, vol. 25, no. 2, pp. 4–36 (Russian).
29. Lorenz, E. N., Deterministic Nonperiodic Flow, *J. Atmospheric Sci.,* 1963, vol. 20, no. 2, pp. 130–141.
30. Sparrow, C., *The Lorenz Equations: Bifurcations, Chaos, and Strange Attractors,* New York: Springer, 1982.
31. Schuster, H. G. and Just, W., *Deterministic Chaos: An Introduction,* Weinheim: Wiley-VCH, 2005.
32. Frøyland, J. and Alfsen, K. H., Lyapunov-Exponent Spectra for the Lorenz Model, *Phys. Rev. A,* 1984, vol. 29, no. 5, pp. 2928–2931.
33. Kuznetsov, S. P., *Dynamical Chaos,* 2nd ed., Moscow: Fizmatlit, 2006 (Russian).
34. Bykov, V. V. and Shil'nikov, L. P., On the Boundaries of the Domain of Existence of the Lorenz Attractor, *Selecta Math. Soviet.,* 1992, vol. 11, no. 4, pp. 375–382.
35. Rössler, O. E., An Equation for Continuous Chaos, *Phys. Lett. A*, 1976, vol. 57, no. 5, pp. 397–398.
36. Gonchenko, S. V., Ovsyannikov, I. I., Simó, C., and Turaev, D., Three-Dimensional Hénon-Like Maps and Wild Lorenz-Like Attractors, *Internat. J. Bifur. Chaos Appl. Sci. Engrg.,* 2005, vol. 15, no. 11, pp. 3493–3508.
37. Hunter, J. D., Matplotlib: A 2D Graphics Environment, *Comput. Sci. Eng.,* 2007, vol. 9, no. 3, pp. 90–95.
38. Smale, S., Differentiable Dynamical Systems, *Bull. Amer. Math. Soc.,* 1967, vol. 73, no. 6, pp. 747–817.
39. *Dynamical Systems 9: Dynamical Systems with Hyperbolic Behaviour,* D. V. Anosov (Ed.), Encyclopaedia Math. Sci., vol. 66, Berlin: Springer, 1995.
40. Shilnikov, L. P., Shilnikov, A. L., Turaev, D., and Chua, L. O., *Methods of Qualitative Theory in Nonlinear Dynamics: Part 2,* World Sci. Ser. Nonlinear Sci. Ser. A Monogr. Treatises, vol. 5, River Edge, N.J.: World Sci., 2001.
41. Gonchenko, S. V., Kazakov, A. O., and Turaev, D., Wild Pseudohyperbolic Attractors in a Four-Dimensional Lorenz System, *in preparation* (2018).
42. Borisov, A. V., Kazakov, A. O., and Sataev, I. R., Spiral Chaos in the Nonholonomic Model of a Chaplygin Top, *Regul. Chaotic Dyn.,* 2016, vol. 21, nos. 7–8, pp. 939–954.
43. Aston, Ph. J. and Laing, C. R., Symmetry and Chaos in the Complex Ginzburg – Landau Equation: 1. Reflectional Symmetries, *Dynam. Stabil. Syst.,* 1999, vol. 14, no. 3, pp. 233–253.
44. Aston, Ph. J. and Laing, C. R., Symmetry and Chaos in the Complex Ginzburg – Landau Equation: 2. Translational Symmetries, *Phys. D,* 2000, vol. 135, no. 1, pp. 79–97.